



ADDIS ABABA UNIVERSITY  
ADDIS ABABA INSTITUTE OF TECHNOLOGY  
SCHOOL OF MECHANICAL AND INDUSTRIAL ENGINEERING  
(MECHANICAL DESIGN STREAM)

---

**NUMERICAL MODELING OF MODE II SUBSURFACE CRACK  
PROPAGATION OF THROUGH-HARDENED Fe-0.5Mo-4Ni-2Cu-0.6C  
STEEL SUBJECTED TO ROLLING–SLIDING CONTACT**

---

A MASTERS THESIS SUBMITTED TO SCHOOL OF MECHANICAL AND  
INDUSTRIAL ENGINEERING OF ADDIS ABABA UNIVERSITY IN PARTIAL  
FULFILLMENT OF THE REQUIREMENTS FOR THE AWARD OF DEGREE OF  
MASTERS OF SCIENCE (MSc.) IN MECHANICAL DESIGN.

By: Heaven Gofawork Assefa

Advisor: Dr. Samuel Tesfaye

May 2021

ADDIS ABABA UNIVERSITY  
ADDIS ABABA INSTITUTE OF TECHNOLOGY  
SCHOOL OF MECHANICAL AND INDUSTRIAL ENGINEERING

**NUMERICAL MODELING OF MODE II SUBSURFACE CRACK PROPAGATION  
OF THROUGH-HARDENED Fe-0.5Mo-4Ni-2Cu-0.6C STEEL SUBJECTED TO  
ROLLING-SLIDING CONTACT**

By

**Heaven Gofawork Assefa**

**Approved by the board of examiners**

**Samuel Tesfaye(Ph.D.)**

Advisor



Signature

Date

**Mulugeta Habtemariam(Ph.D.)**

Exterenal Examiner

Signature

Date

**Araya Abera (Ph.D. candidate)**

Internal Examiner

Signature

Date

**Araya Abera (Ph.D. candidate)**

Mechanical design Chairman

Signature

Date

**Yilma Tadesa(Ph.D.)**

SMIE Dean

Signature

Date

**Ermias Tesfaye (Ph.D.)**

Director of Postgraduate

Signature

Date





## **Acknowledgment**

First of all, I am extremely grateful to my advisor, Dr. Samuel, Assistant Professor at the Addis Ababa Institute of Technology, for his immense knowledge and abundant experience that has helped me throughout academic research. Last, I would like to express my gratitude to my parents. Without their wonderful understanding and encouragement, it would be impossible.

## ABSTRACT

Contact fatigue is the main damage mechanism of the mechanical components that are subjected to cyclic contact stresses. Gears, bearings, and cams are among the components that may fail due to contact fatigue or subsurface crack propagation. Subsurface crack propagation is affected by contact loads, contact surface frictions, the presence of asperity contacts, and initial crack direction parameters. In this research work, the effect of load, crack angle, and contact surface coefficient of friction on subsurface crack propagation and stress distribution was analyzed using a numerical approach. An extended finite element method (XFEM) was employed to study stress distribution and crack propagation. The investigation focused on the understood crack propagation using the numerical approach as it was predicted using theoretical analysis and observed during the experimental test of through-hardened steel. After inserting the initial crack at a depth (at the depth  $z$  where shear stress is maximum when we apply 622 MPa pressure) from the surface with a 2D plane strain condition. The result showed that subsurface crack propagation was dependent on the load, crack angle, and surface coefficient of friction: it grows linearly with load; decreases with increasing of surface friction coefficient; and maximum crack propagation is obtained at 45 degrees of crack angle. Again, as the applied pressure, coefficient of friction, and crack angle varies, the position of the maximum equivalent stress (nucleation site). The material for a mean pressure of 622 MPa causes cracks to propagate to 37.973  $\mu\text{m}$  and when compared to the experimental crack length has a percentage of error of 5.067%. The comparison between the numerical results and the given experimental result shows reliability at a pressure of 622MPa.

*Keywords: - Through hardened steel, Rolling-sliding contact, Subsurface crack propagation, Numerical modeling*

## TABLE OF CONTENTS

<b>DECLARATION.....</b>	<b>IV</b>
<b>ACKNOWLEDGMENT .....</b>	<b>V</b>
<b>ABSTRACT.....</b>	<b>VI</b>
<b>TABLE OF CONTENTS .....</b>	<b>VII</b>
<b>LIST OF TABLES .....</b>	<b>IX</b>
<b>LIST OF FIGURES .....</b>	<b>X</b>
<b>LIST OF EQUATION.....</b>	<b>XI</b>
<b>ABBRAVATION.....</b>	<b>XII</b>
<b>NOMENCLATURE.....</b>	<b>XIII</b>
<b>CHAPTER -1 INTRODUCTION .....</b>	<b>XIII</b>
1.1 Introduction .....	1
1.2 Statement of the problem .....	4
1.3 Objective .....	5
1.3.1 General objective .....	5
1.3.2 Specific objective.....	5
1.4 Significance of the study .....	5
1.5 Scope of the study .....	5
<b>CHAPTER -2 LITERATURE REVIEW .....</b>	<b>6</b>
2.1 Based on Contact Mechanics .....	6
2.1.1 Based on the Effect of Load .....	7
2.1.2 Based on the Effect of Friction and Lubrication .....	8
2.1.3 Effect of Material Property .....	10
2.2 Rolling –Sliding contact.....	13
2.3 Fatigue Contact and Crack .....	14
2.4 Surface crack .....	16
2.5 Sub-Surface Crack.....	17
2.6 Numerical Analysis .....	18
2.7 Summary .....	19

<b>CHAPTER - 3 MATHEMATICAL MODELING AND METHODS .....</b>	<b>20</b>
3.1 Materials.....	20
3.2 Mathematical Modeling of Subsurface crack.....	22
3.2.1 Crack nucleation .....	22
3.3 Finite element modeling of contact mechanics and crack propagations .....	25
3.4 Numerical modeling of contacting elements using Abaqus.....	28
3.4.1 Crate Part .....	28
3.4.2 Material property section.....	28
3.4.3 Assembly section.....	29
3.4.4 Step section.....	29
3.4.5 Interaction section.....	30
3.4.6 Boundary condition and load application.....	31
3.4.7 Meshing .....	32
3.4.8 Job, Simulation and post-processing .....	34
<b>CHAPTER - 4 RESULT AND DISCUSSION .....</b>	<b>35</b>
4.1 The effect of load on the stress distribution .....	35
4.2 The effect of contact surface friction on stress distribution .....	36
4.3 The Effect of crack angle on the stress distribution .....	38
4.4 Crack propagation .....	39
A. The effect of applied load on propagated crack length.....	39
B. The effect of surface friction on the crack propagation.....	41
C. The effect of crack angle on crack propagation.....	42
4.5 Validation using the experimental results .....	45
<b>CHAPTER - 5 CONCLUSIONS AND RECOMMENDATIONS.....</b>	<b>47</b>
5.1 Conclusion.....	47
5.2 Recommendation.....	47
5.3 Future work .....	48
<b>REFERENCES.....</b>	<b>49</b>

## LIST OF TABLES

Table 3. 1 Parameter of the material of the object .....	21
Table 3. 2 Material property of slave disc object.....	22
Table 3. 3 System unit in Abaqus .....	27
Table 3. 4 Dimensions of master and slave disc .....	28
Table 3. 5 Material property of master and slave disc .....	29
Table 3. 6 Static model analysis parameters .....	30
Table 3. 7 Tabular presentations of amplitude through the steps .....	30
Table 3. 8 Contact type and property .....	31
Table 3. 9 Boundaries and load condition .....	32
Table 3. 10 Parameters of mesh convergency .....	33
Table 3. 11 Mesh property of master and slave disc.....	34
Table 4. 1The effect of load on the depth of maximum shear stress exists .....	35
Table 4. 2 Error percentage of crack propagation.....	46

## LIST OF FIGURES

Figure 1.1 Gear .....	3
Figure 1. 2 Examples of surface damage of gear teeth and roller .....	3
Figure 1. 3 Crack initiation and propagation tested at 622 MPa mean pressure .....	4
Figure 3. 1 schematically representation of the body .....	20
Figure 3. 2 Modes of fracture .....	23
Figure 3. 3 Methods crack analysis.....	27
Figure 3. 4 master disc modeling & Figure 3. 5 slave disc modeling .....	28
Figure 3. 6 Assembly model of master and slave disc.....	29
Figure 3. 7 Mode of simplification rolling sliding contact to sliding contact.....	31
Figure 3. 8 The finite element mesh of the object .....	32
Figure 3. 9 Mesh convergence analysis .....	33
Figure 3. 10 Summary of numerical analysis .....	34
Figure 4. 1 The effect of load on the distribution and depth of maximum shear stress exists.....	35
Figure 4. 2 Shear stress distribution with different coefficient of friction without initial crack ...	36
Figure 4. 3 Shear stress distribution with different coefficient of friction with initial crack. ....	37
Figure 4. 4 Contour map of equivalent stress distribution at the 622 MPa pressure and 0.17 coefficient of friction. ....	38
Figure 4. 5 Shear stress distribution with different Crack Angle .....	39
Figure 4. 6 crack length and the influence of applying pressure .....	40
Figure 4. 7 The contour map of maximum stress distribution around the crack tip.....	41
Figure 4. 8 the effect of surface friction of the crack propagation .....	41
Figure 4. 9 The contour map of equivalent stress distributions prepared by applying a load of 622 MPa pressure and for the coefficient of friction of 0, 0.1, and 0.3.....	42
Figure 4. 10 The effect of crack angle on the crack propagation .....	43
Figure 4. 11 The contour map of equivalent stress distributions prepared by applying a load of 622 MPa pressure and for the crack.....	43
Figure 4. 12 The output of crack propagation with increasing cyclic load.....	44
Figure 4. 13 mean pressure and crack initiation of experimental data .....	45
Figure 4. 14 Crack propagation analyzed using the numerical method by applying 622 MPa mean pressure, 45-degree crack angle, and 0.17 coefficient of surface friction.....	45

**LIST OF EQUATION**

Equation 3. 1 .....23  
Equation 3. 2 .....23  
Equation 3. 3 .....23  
Equation 3. 4 .....23  
Equation 3. 5 .....24  
Equation 3. 6 .....24  
Equation 3. 7 .....24  
Equation 3. 8 .....24

## ABBRAVATION

CPE4R	Quadrilateral, reduced integration element
CTOD	Crack tip opening displacement
CZM	Cohesive zone model
EPFM	Elastic-plastic fracture mechanics
FEA	Finite element analysis
FEM	finite element method
LEFM	linear elastic fracture mechanics
LSM	Level Set Method
MAXE	Maximum nominal strain criterion
MAXPE	Maximum Principal strain criterion
MAXPS	Maximum Principal stress Criterion
MAXS	Maximum nominal stress Criterion
MTS	Maximum tangential stress
PM	pressurization mechanism
QUADE	Quadratic Nominal strain
QUADS	Quadratic Nominal strain
RCF	Rolling Contact Fatigue
RSCF	rolling sliding contact fatigue
SIF	stress intensity factor
VCCT	Virtual crack closure technique
WFM	Weight Function Method
XFEM	extended finite element method

## NOMENCLATURE

$a_0$	Initial Crack length [ $\mu\text{m}$ ]
$\alpha$	Crack inclination angle [ $^\circ$ ]
$\nu$	Poisson's ratio [-]
$\mu$	Contact surface friction [-]
$\sigma_y$	Yield strength rate [MPa]
$a$	Crack length [ $\mu\text{m}$ ]
$b$	Hertzian contact pressure distribution half-width [mm]
$E_c$	Elastic modulus [ $N/mm^{0.5}$ ]
$G$	Energy release rate [N/ m <sup>2</sup> ]
$G_{Ic}$	Fracture energy rate [N/mm]
$F_f$	Friction force [N]
$F_N$	Normal force [N]
$J$	J- integral [-]
$K_{II}$	Mode II SIFs [MPa $\sqrt{\text{m}}$ ]
$K_{Ic}$	Fracture toughness rate [MPa $\sqrt{\text{m}}$ ]
$P$	Hertzian pressure on the surface [MPa]
$P_{\text{max}}$	Maximum Hertzian contact pressure distribution [MPa]
$R_c$	Effective radius [mm]

## CHAPTER 1 INTRODUCTION

### 1.1 Introduction

Machine components such as bearings, gears, cam, and its followers, etc. are frequently subjected to high contact loads and high operating speeds. These loading and running conditions applied on the elements undergo rolling sliding contact tend to deform elastically (Elasto hydrodynamic) and then deforms plastically up to the final resistance of the materials or up to fracture. Fracture is a problem that for a long time has been faced by society. Today, the problem is getting worse because they use the higher load for heavily loaded applications that need support. Many complex engineering components are rolling-sliding contacts, such as gears, cams, and their followers, bearings, etc. [1].

The life of the material, which is subjected to high rolling-sliding contact load, is directly related to the surface characteristics, running speeds, and lubrication conditions. The contact surface zone is small and there is a higher pressure that typically results in the fracture of the contact surfaces. In particular, if the contact load is cyclic, the failure could occur at lower stress, which is obvious for most components[2].

A phenomenon that can cause different engineered structures to fail to touch metallic surfaces is rolling sliding fatigue contact. Various types of contact fatigue may occur, including yielding, buckling, brittle and ductile fracture. Stress increases dramatically when a defect is present in the material and that results in the nucleation of cracks and then grows to a critical [3].

And where the stress has been reduced, either a gradual crack from the extreme surface or the contact interface below may cause the fracture to occur. Mechanical components experience rolling sliding contact with elevated contact loads at the rolling contact. Due to the fatigue of rolling sliding contact, various structural components of engineering commonly suffer from cracks on the touch surface.

A surface hole forming type damage is usually found in a ball or roller bearings that are distinguished as contact fatigue. Similarly, it is found in mechanical equipment such as gears, cams, valves, rails, and gear couplings. Contact fatigue has been differentiated in combinations of two or more elements at least one of which is a metal. The difference between contact fatigue and other fatigue is that contact fatigue results from contact or Hertzian stress state. As a result, the materials in a specific area that are in stress state curved surfaces are in contact under a normal load [4].

The first case is when one surface moves over the other in a rolling motion as in a ball rolling over a race in a ball bearing that means both the mate parts are move and the second one is sliding contact of the component when two bodies have sliding contact that means one body moves and the other one

stationary. The contact geometry and the motion of the rolling sliding elements produce an alternating subsurface shear stress. Subsurface materials strain accumulates with growing upcycles until a crack is generated. The crack then propagates until a pit is formed. Once surface damage or pit has been started, the bearing becomes clamorous and uneven operating.

If it is allowed to continue, damage to the rotating material and disastrous damage occurs. A damaged variety of components can result from fatigue breaking and high hoop stresses. Rolling contact components have a material failure life such as cracking or separation, caused by stress on the components. When assessing, structural fatigue has an endurance limit over contact fatigue. If one analyzes the difference, similarities, and fatigue lives of cyclic torsion with rolling contact, the latter is exceeding by seven orders of magnitude [5].

A crack is a break or gap in a strong body which is determined by giving a starting or nucleation point and, by increasing from this point to limited size with time, either leading or not, to the division of the initial body in two or more pieces here are some of the figures about crack affecting material. Contact fatigue cracks nucleation and growth, typically studied with the help of numerical models using the fracture mechanic approach. In fracture mechanics, many numerical techniques have been generated and applied, such as the finite element system, the finite difference method, etc. [5].

Of all numerical methods, the FEM and XFEM are the most widely used. Because of its ability to deal with the difficult geometries and complex boundary conditions undoubtedly, as a means of solving realistic engineering fracture issues. A general 2-D crack propagation model is generated using both traditional FEM and XFEM methods for modeling crack propagation. The Finite Element Approach has been used for the past few decades to assist engineers in the study of the most complicated structures. Until recently, it was essential to model cracks as part of the geometry of the structure. As the crack expanded, the model would be rebuilt and re-meshed, requiring essential user interaction or specialized programs.

To understand the nucleation and propagation of surface and subsurface crack in the materials subjected to the contact load, figure 1.2 represents examples of real component (gear teeth and roller) failure during their functionality.

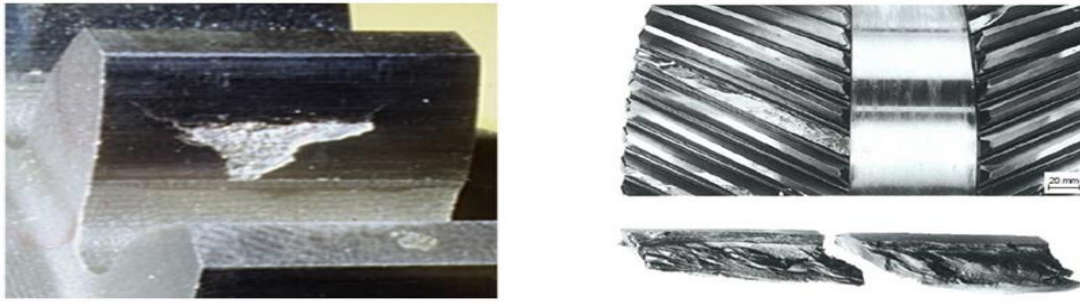


**Figure 1.1** Gear [6]



**Figure 1. 2** Examples of surface damage of gear teeth and roller [7]

Depending on the surface characteristics, contact conditions, and geometry of the components, the crack may nucleate either at the surface or subsurface before propagation to produce the final surface detachment. The study of crack nucleation and propagation can be approached using analytical, numerical, and experimental methods. The nucleation of surface and subsurface crack in the microstructure through-hardened powder metallurgy material (Fe-0.5%Mo-4%Ni-2%Cu-0.6%C) were analyzed using a Hertzian model, and the prediction was validated using the ring-on-ring wear damage tests. Figure 1.3 shows the analytical predictions based on the local approach (comparing the resistance of each constituent of the material with the applied equivalent stress) and validated using contact fatigue results after testing at different pressures (crack propagation occurs at 622 MPa) applied to mean Hertzian pressure [8].

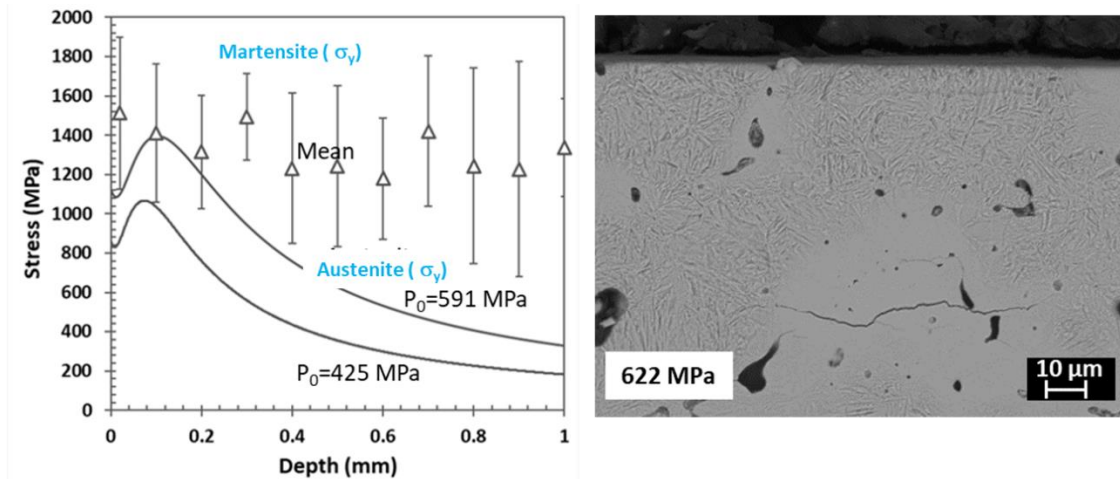


**Figure 1. 3 Crack initiation and propagation tested at 622 MPa mean pressure[8]**

The analytical model shows that failure may start at different applied mean pressure based on martensite microstructure resistance (at 750 MPa), mean resistance (591 MPa), and austenite microstructure resistance (at 425 MPa). The depth of the crack that is observed in the microstructure of austenite as the experimental results is about 100 μm from the surface while it is predicted to be observed below 70 μm (corresponds to the position of maximum stress). In the experimental results, the depth of crack nucleation may depend on many parameters, such as initial crack angle, contact surface friction, and applied load.

In this work, the effect of initial crack inclination, contact surface friction, and applied load on the position and growth of subsurface surface cracks (nucleation and propagation) will be analyzed.

## 1.2 Statement of the problem

Through hardened powder metallurgy steel components are utilized in many machine parts which are subjected to high dynamic contact pressures that result in nucleation and propagation of cracks until final fracture. The contact fatigue crack is initiated somewhere on the subsurface and cannot be observed until they grow to the surface, and the position of nucleation and crack growth direction depends on load, contact surface friction, lubrication, initial crack size and direction, and other parameters. Different researches seek study on crack initiation and propagation due to different condition using the conventional FEM approach but this thesis concern on study crack propagation of through hardened Fe-0.5Mo-4Ni-2Cu-0.6c Steel with an initial crack at the subsurface by using XFEM. The contact fatigue crack investigation is an important research topic in contact mechanics that should be always analyzed for materials because it is a parametric-dependent damage mechanism. So that it is highly demanded to study the crack propagation accurately under the selected parameter and numerical methods have to be used to predict and analyze failure on materials. Therefore, the

investigation of the behavior of subsurface crack propagation in the material is very important to avoid damage and to manage safety. It helps to find the crack resisting mechanism for the materials.

### **1.3 Objective**

#### **1.3.1 General objective**

The general objective of this research is to study subsurface crack propagation of through-hardened steel subjected under rolling – sliding contact using numerical analysis.

#### **1.3.2 Specific objective**

The specific objectives are -

- To study the effect of applied pressure, crack angle, and contact surface friction on the stress distribution and the position of crack initiation.
- To examine the effect of pressure, coefficient of surface friction, and crack angle on the crack propagations.

### **1.4 Significance of the study**

Contact fatigue is one of the damage mechanisms of mechanical components that are subjected to contact loads. The characteristics of a fatigue crack have two parts, initiation and propagation. Crack propagation in which the energy flow from the stress-strain field to the crack edge will be investigated within hardened metal subsurface. Those damages or failures due to the applied pressure on rolling-sliding contact nucleate and propagates within the subsurface can be studied with where crack initiate and how much crack will be propagated. Finally, the investigation gives subsurface crack propagation gives a clue or hint for others how to avoid damages of how to manage safety.

### **1.5 Scope of the study**

Using the finite element method, this research investigates the mode II subsurface fracture of a material subjected to rolling sliding contacting. The fracture energy release rate  $s$  at the crack will be determined, as will the variation of influential parameters such as contacting load, friction, and crack inclination angle. Finally, the numerical results will be compared to the analytical and experimental results obtained in the paper [9]. However, other parameters such as surface roughness, temperature, material type, geometry, and residual stress will not be considered in this work. The crack propagation analysis will only use the XFEM approach and will be limited to homogeneous properties.

## CHAPTER -2 LITERATURE REVIEW

In this chapter reviews of literature surrounding the contact mechanics, rolling-sliding contact, fatigue contact and crack, types of crack, and numerical methods are discussed.

### 2.1 Based on Contact Mechanics

Contact mechanics is the study of material reactions as two bodies come into contact. Contacts between structures can result in very high pressures, which can lead to collapse or fracture. This section discusses the effects of load, friction and lubrication, and material properties on contact mechanics.

Anoopnath P. R. et.al [9] investigated “Hertz Contact Stress of Deep Groove Ball Bearing” and studied calculations of “hertz contact stress between the deep groove ball bearing and inner race.” The method used in this method was analytical and tool analysis. In another meaning, this method was used to forecast the contact force between inner race and ball of single row deep groove ball bearing.

Jiixin Zhao et.al [10] studied a Finite Element Analysis of Surface Pocket Effects in Hertzian Linear Contact. This research article presents the FEA model of a stiff hollow cylinder in contact with stretching and elastic-linear-kinematic-hardening-plastic MESH half-space with lube-filled surface pockets. The results demonstrated by the lubricant that share the load effects successfully with filled pockets and empty pockets

Usman and Shyh-Chour Huang [11] summarized the stress behavior of the contact mechanism in complete knee substitution using two-dimensional FEA in the human body joint by using plastic and elastic body. In this study, the stress behavior in the human body was investigated by FEA, and a two-dimensional FE model representing the knee joint contact mechanism was created. Finally, the comparison between elastic and plastic knee joints was created to observe the performances.

R. Ledesma-Alonso et.al [12] studied a simple model to describe the “Boussinesq–Cerruti like contact between the lens and a single stretching pillar”, which assumes the pillar geometry and the elastic properties of the two bodies. The method utilized in this research is numerical methods or superposition method and an iterative bisection like method. A change from one form to another between “the limiting contact regimes, Hertzian and soft-flat-punch”, is well described by a rational function.

Ling Wang et.al [13] investigated the individual and combined effect of the “cup inclination and wear on the contact mechanics and fixation” of a human body hip substitution using FEM. Here, the effects of contact mechanics, the force within the cement, and at the bone–cement interface were inspected carefully. Finally, the result shows very high contact pressure, and the Von Mises stress on the cup were decreased when even a small movement from one place to another occurred and contact

mechanics, the cement stress is unaffected or not showing variation to the cup inclination and wear under these normal conditions which explaining the very strength of the Charnley hip implant.

Z.-Q. Gong and K. Komvopoulos [14] demonstrated the effect of plain-strain FEA for elastic-plastic layered median order to explain the effect of surface geometry on the deformation and stress field due to normal and sliding contact. The modeling of Surface interaction between the layers is used for more illustrations. Finally, for different surfaces, the consequences are contrasted based on the contact pressure distribution, surface tensile stress, and subsurface equivalent plastic strain and predictions for the developed yield criterion and obtained finite element simulations analyzed.

### **2.1.1 Based on the Effect of Load**

Deformation in contact mechanics is concerned with pressures applied to the body. The contact may be conforming or nonconforming. Conforming interaction occurs as the surfaces of two bodies fit perfectly or quite precisely without deformation. Non-conforming contact is described as the touch between bodies with dissimilar profiles. In this topic, the effect of applied load on contact mechanics is reviewed.

Wei Wang et.al [15] examined the result of load on tribological properties of silicon nitride steel under the action of rolling sliding contact. The material's behavior under various weights was studied by using a modified rolling-sliding contact device. Finally, the results showed the comparison between pure sliding friction contact and rolling-sliding contact condition with parameters of friction coefficient and the wear rate.

H. Long et.al [16] investigated the subsurface and surface crack initiation under rolling and surface sliding contact fatigue for turbine gearbox bearings. The method or the tests utilized in this research was “white etching crack networks and twin-disc rolling contact fatigue test for testing premature failure of the bearings.” Finally, the determined parameters for the cracks are the starting or initial stages of contact pressure, surface traction, and impact loading required for the structure of inclusion-initiated micro-cracks and white etching area.

M. Khajeh Salehani al et. [17] Examined adhesive contacts under tangential loading. Both software simulation and experimental study were carried out to study how the contact area and tractions of an adhesive circular smooth punch evolve under mixed-mode loading, before and after sliding. “Green’s function molecular dynamics” method is used to describe the interactions between contacting bodies through tension, compression, and shear. In both simulation and experimental observations, the decrement in the meeting area during shear loading is found to be symmetric under tension and asymmetric under compression.

D.I. Fletcher and J.H. Beynon [18] investigated “the effect of contact load reduction on the fatigue life of pearlitic rail steel in lubricated rolling–sliding contact.” Three Mechanism (TM) models have been used in this research. The testing materials to test the efficiency of the design and the model of contact pressure variation on rail steel fatigue life is twin-disc contact simulation tests. The lubricants used were an oil carrier fluid and water. For both types of lubricants, the reduction of the maximum Hertzian contact pressure extended the fatigue life of the rail steel by over five times however water lubrications produced only a marginal increase in fatigue life.

### **2.1.2 Based on the Effect of Friction and Lubrication**

Friction is the force that resists the relative motion of rigid plates, fluid layers, and material components sliding against one another. There are two forms of friction: dry friction and fluid friction. Metal flat rolling focuses on two interconnected phenomena: friction and lubrication at the contact surfaces. Friction and lubrication's effects on contact mechanics are discussed.

B. J. Briscoe and F. Motamedi [19] proposed “the ballistic impact characteristics of aramid fabrics and the influence of interface friction based on the effect of the surface friction behaviors of aramid fabrics concerning their static deformation behavior and their ballistic capture performance.” A simple very narrow stretching plate model was used to describe barely the quasi-static response of the fabrics to an original indentation deformation. A simple simulation was invented for the first-order model of the quasi-static indentation process. The predicted results of the relative fabric ballistic captive efficiency and filament-filament with yarn-yarn junctions, derived from this model, were found to be in a safe agreement with the results acquired directly from the ballistic studies.

Gema Styles et.al [20] investigated “cycle and life-time friction transience in piston ring–liner conjunction under the mixed regime of lubrication”. The Greenwood, Reynolds equation, and Tripp model are used to predicting asperity-level contribution to total piston friction. The merging of graphic representation and coating behaviors important to develop the essential variables for a boundary friction model. Based on the lubrication called “mixed-hydrodynamic regime”, a numerical model of the top compression ring to cylinder line is developed. The result of friction and coating on the power loss and wear of the conjunction are explained to forecast the life span of the piston ring-liner.

D.E.Sander et.al [21] studied the friction behaviors of journal bearings operating from hydrodynamic to mixed lubrication ways where a lot of metal-metal contacts occur. Two different static loads are applied to the journal bearing to test the contact friction. The “Greenwood and Tripp contact” model was considered to derive surface parameters from surface scans. The test results in form of Strobeck curves give a good approach to test the isothermal Electrohydrodynamic simulation approach.

B. N. J. Person[22] investigated “how the friction force depends on the nature of the substrate surface roughness and the sliding velocity.” In a theory of friction, when rubber moves on a rough surface, the surface harshness of the substrate exert back and forth forces on the rubber surface it driving away from the energy via the innermost friction of the rubber. The consideration has been taken place in detail when the substrate surface has a self-affine fractal structure and also another thing presented is a theory for the area of real contact, both for stationary and sliding bodies, with elastic or elastoplastic properties. The theoretical results are in good agreement with experimental observation.

Xiang-dong Chang et.al [23] studied the “friction and wear properties of steel wire rope sliding against itself under impact load.” To attribute the meaning of friction and wear mechanisms of wire rope among the layers in the winding hoist, various sliding friction experiments were executed using a self-made friction test rig. The consequences imply that the coefficient of friction of the wire rope varies little with increase load and stabilize, but decreases with the sliding velocity under dry-friction condition.

J.D.B. de Mello et.al [24]investigated the abrasive wear mechanisms of rolling and at the same time sliding active particles. The superimposition of the principle of the interaction at the wear interface has been used. Similarly, “single abrasive particle interactions are simulated using well-controlled indentation or scratch tests.” The results clearly showed a change from one form to another in the wear mechanisms when the degree of superimposition was changed for both the indentation and the scratch tests.

J.R. Barber et.al [25]elucubrated the cause of plasticity on fretting wear. The model used was a finite-element model. The permanent change in the size of materials when the stress is applied adds another dimensionless parameter into the analysis, but the results of considerable generality can still be kept. In particular, the final effect shows that the contact pressure distribution shows the maximum accumulated plastic strain go up closely linearly with the number of loading cycles and occurs close to the instantaneous slip-stick boundary.

S. Fouvry et.al [26] studied crack nucleation using fatigue criteria in the case of an elastically stressed not lubricated contact. Fretting behavior is differentiated in the manner of experiment and analysis which means transition criteria created with the help of Midline’s analysis. Similarly, a “Dang Van crack nucleation criterion” is introduced for a ball-flat contact. Typical analytical parameters of the criterion were described as a function of the mechanical properties, the friction coefficient, the contact geometries, and the fatigue limits for both shear and tensile loading of the material. The results gained permit the investigation of the position and the direction of the first crack created by fretting conditions.

Wei Cao et.al [27] investigated the “effect of contact path on the combined lubrication characteristics, friction and contact fatigue in spiral bevel gears” with taking account of surface roughness. Overall analysis for gearing geometry, kinematics, and contact load with various contact paths processed based on the loaded tooth contact analysis. By using a mixed EHL model for spiral bevel gears the corresponding lubrication parameters which are friction coefficient, flash temperature, and fatigue life are carried out in a large range of working conditions. Obtained results show that the contact path is very essential to lubrication performance, efficiency improvements, and fatigue prevention.

Sorin-Cristian Valdes et.al [28] investigated mixed friction and wear decrement in a reciprocating contact through laser surface texturing. The aim is to briefly understand the effect between laser-textured surface pockets and friction and wear behavior of the vehicle piston-liner pairing. To apply the procedure, a newly developed, and reciprocating, test apparatus was used to conduct wear tests under highly loaded conditions. These tests revealed that as the object for analysis becomes damaged and surface roughness goes up, the contact progresses further into the mixed and boundary regime.

K.W. Liew et.al [29] investigated the “cause of electrical discharge machined dimple geometry on friction reduction under boundary and mixed lubrication.” The samples were examined in a contrary to a revolving high-speed steel counter-disc using a pin on disc set-up under mixed lubrication condition. Tribo-tests were carried out at growing up sliding speed with changing nominal contact pressures. Finally, it is verified that the round dimple geometry gives the lowest friction and wear among others.

Oskari Elomaa et.al [30] studied the comparison of the graphene oxide in water lubrication on diamond-like carbon and stainless steel high-load contacts. The wear surfaces of the materials were characterized using the following parameters such as contact profilometry, X-ray spectroscopy, optical microscopy, scanning electron microscopy, energy dispersive spectroscopy, and Raman spectroscopy. The comparison parameter used in this research is the coefficient of frictions. The friction coefficient was reduced compared to pure water when similar graphene oxide and normal load were applied. The smallest amount of wear for the counter ball was examined when pure water was used. The graphene oxide additives used in this research reduced the corrosive cause on the counter ball.

### **2.1.3 Effect of Material Property**

Material properties such as yield strength, poissons ratio, young’s modulus. etc. have their impact on contact mechanics, so the effect of material properties is discussed

S. Suresh et.al [31] elucidated the effects of metal to metal properties and surface friction on Elasto-plastic sliding contact. The frictional sliding practical proof was executed with the help of a

Nanoindentation testing system, where grain size and alloy composition were found to affect the response. Finally, the results revealed that an increase in the strain hardening exponent can decrease in a large amount of the pile-up height, with known and further potential implications for the evaluation of tribological damage.

A. Papangelo and M. Ciavarella [32] studied the “contact area reduction under shear load in soft materials.” The model applied was mixed-mode fracture mechanics for wholly brittle’ model of Savkoor and Briggs, models have been proposed and compared with two such previously proposed models and introduce a third one to show that the transition to sliding is very sensitive to the form of the mixed-mode model. Finally, it is concluded that the unstable points are different under load or displacement control. Hence, the form of the mixed-mode function, and not only in parameter, is an extremely sensible choice.

M. L. Dumont et.al [33] elucidated the role of inclusions, surface roughness, and operating conditions on rolling contact fatigue. Experimental tests have been performed on a two-disk machine of two bearing plates of steel. The operating conditions have been selected to describe typical jet engine applications. By applying the rolling contact fatigue theories, the experimental results are analyzed and discussed. Surface damage and sub-surface damage which could result in disastrous failure have been observed.

Eralp Demir and Dierk Raabe [34] studied the mechanical and microstructural Bauschinger effect on a curved material and not crooked a very small-sized single-crystal copper beam over three consecutive cycles. Bauschinger two effects have been observed such as the internal back stresses and the decreased criteria to turn on dislocation soakage during backloading as the dislocations. Finally, the yield stress falls and the degree of microstructure reversibility upon load path changes is described.

J.Y vonnet et.al [35] investigated crack nucleation and propagation in strongly different materials at a microstructure level. In this study, a phase-field model method and highly heterogeneous materials model method used to simulate crack initiation and propagation in the 2D and 3D methods. The miscellaneous advantages of the phase-field method for voxel-based models are demonstrated. Finally, it is verified that the resolution related to the initial image and thus to meshes for separating the same microstructure does not importantly affect the simulated crack path.

Daw-Kwei Leu [36] studied the modeling of surface coarseness effect on dry contact friction in metal forming. The developed model was a dry friction model that accounted for the adhesion and interference effects of surface coarseness. The model explained in this investigation was verified by previously published experiments and predicted values which is an effective convention with

experimental results. Simulations verify that the friction coefficient is reduced as dimensionless stress goes up at a small strain hardening exponent.

Nazife Erarslan [37] elucidated “microstructural investigation of subcritical crack propagation and fracture process zone (FPZ).” For a more detailed study, diametrical compression tests and Brisbane tuff disc specimens were performed. The mode-I (tensile) fracture toughness (K<sub>IC</sub>) response to static and cyclic loading is used to test rocks under mechanical loading without a corrosive chemical environment. It is verified that the rock texture behavior such as interlocked and cemented grains, cement volume, cement mineralogy has a great role in the destructive behavior of rocks and improvement of FPZ and subcritical cracking.

Marcelo Epstein and Ayan Roy Chowdhury[38] investigated the embedded homogeneity of beams in the indirect domain. An invention of embedded homogeneity of thin-walled structures is illustrated in detail as the property characterizing the provenance of such a structure from a homogeneous material. Good conditions for embedded similarity are manifested for planar beams and their geometric definition is explained as the condition for the elastic hodograph to lie on a hypersphere containing the origin of a six-dimensional space of tensors.

Kenneth R. Gratz et.al [39] investigated the “effects of focal joint fault on cartilage contact mechanics.” The purpose of this research was to clarify the effect of experimental full-thickness focal defects, oriented at a specific value which is relative to the subchondral bone, on the inter issued strain and surface sliding of opposing cartilage surfaces during compression and stress relaxation. The results point out that the loading of intact samples will cause axial strain magnitudes that are reduced with depth and relatively little sliding.

L. Galda et.al [40] studied the effect of small indentation geometry in the sliding surface on the tribological properties under emaciated lubrication conditions. In this research, the final evaluation and examinations of sliding pairs in material contact of steel–steel are presented. The tribological test which is called tester pin-on-disc with the modified sliding pair geometry has been demonstrated and the friction coefficient was used as the measuring parameter. Finally, the presence of small indentation on the surface enhanced the tribological characteristics under emaciated lubrication conditions at low sliding speeds.

F. Restagno and J. Crassous [41] proposed the “measurements of the adhesion load between surfaces of Pyrex having a very small coarseness, with a surface force equipment. It is found out that the adhesion force relies on the maximal load that has been applied on the surfaces but does not rely on the time during which they have been in contact. And, finally, a model of plastic deformation of the small asperities in a macroscopic Hertz contact is in good agreement with the experimental data.

G.A.Rogerson et.al [42] investigated the separation phenomena in uniform pre-stressed layered elastic structures. The separation relation related to a similar three-layer structure, made of compressible, pre-stressed elastic layers, is obtained. Mathematically illustrate transcendental equation and numerical solutions confirmed to result in phase speed as an implicit function of wavenumber and to verify a large scope of dispersion characteristics which is exquisitely dependent on the material parameters and pre-stress in each layer respectively. It is proved that these approaches may demonstrate helpful to approach numerical truncation errors associated with impact response, as well as giving good initial approximations for numerically challenging sets of material parameters.

## **2.2 Rolling –Sliding contact**

When two spinning mechanical components come into contact with each other, the contact may be pure rolling, rolling-sliding, or sliding, depending on the relative velocity of the touching bodies. Absolute rolling contact happens at the pitch points of the involute profiles of the teeth in the case of gear tooth contacts so there is no relative velocity at the pitch point. However, slippage or slipping happens as a result of due to relative velocity at the other contact situations along the path of contacts. As a result, the rolling contacts on the gear teeth are essentially sliding contacts. Bearings and other electronic parts are often subjected to rolling sliding touches. To classify contact fatigue behavior, these types of contacts are often experimentally analyzed using a two-disc wear machine. The focus of this segment is on rolling-sliding interaction.

W.J. Qin and C.Y. Guan [43] investigated “contact stresses and crack initiation in spur gears based on finite element dynamics synthesis.” This research uses the contact fatigue main failure mode analysis to study the cyclic load on the materials. The Hertzian theory and finite element method have been utilized to study surface and subsurface stresses of gear teeth. The loads near the engagement and recess areas are resulted in exceeding the static contact conditions and thus found to be in low fatigue life. Similarly, the stress at the tip relief of gear teeth is decreased and improved fatigue life initiations.

Kuhn Zhou and Fei Shen [44] investigated the “effects of the contact pressure and the coefficient of friction on the spalling process in rolling bearings.” An elastoplastic-damage model to study the spalling initiation and propagation characteristics of bearings under rolling contact fatigue loading has been developed. Moreover, the damage-caused plastic deformation causes the shear stress-strain curve to control the hysteresis loop and the fatigue damage emulates with the plastic deformation to act upon the shear stress that plays a great role in spalling.

Matteo Benedetti et.al [45] investigated “fluid pressurization and entrapment effects on the SIFs of Cracks generated under lubricated Rolling-Sliding Contact Fatigue.” The contact load is not

approaching as regular by an analytical pressure distribution but the actual pairing body is modeled. The crack between the pairing bodies via hydrostatic elements is modeled. Here the effect of crack propagation due to lubricant within crack is more investigated.

M. Sraml et.al [46] proposed a mathematical procedure for forecasting the rolling contact fatigue crack initiation. The utilized models are the computational numerical model for contact fatigue damage analysis of mechanical elements and Coffin–Manson relations between deformations and loading cycles. The results that concern the distinguishing of important material points and the number of loading cycles, required for initial fatigue failure to appear at those points, are the basic purpose of the proposed study.

Rahul Raga et.al [47] elucidated “experimental and numerical investigation of crack initiation and propagation in silicon nitride ceramic under rolling and cyclic contact.” The main study area was to investigate the crack initiation and propagation process in silicon nitride which passes through non-conforming hybrid contact under diverse tribological conditions. To understand the predominant modes of failure in silicon nitride, two different model experiments were proposed, namely, rolling contact and cyclic contact experiments.

Potocnik R. et.al [48] demonstrated a parametric study of the “crack growth in the smooth-rolling sliding contact problems.” A two-dimensional mathematical model is used to illustrate the crack direction of proceeding in the smooth rolling-sliding contact problems. The model takes into account that the crack initiation in the first stage of the surface of the gear tooth flank. Different load cases are used to simulate the moving of a contact load. The crack propagation direction of proceeding is evaluated by a maximum tangential stress criterion and modified the maximum tangential stress criterion. The analytical output demonstrates that the consideration of the tangential stress has a significant impact on the crack path in the lubricated rolling-sliding contact problems.

Simone Ancelotti et.al [49] investigated the “function of the component on the pressurization and entrapment of oil in cracks generated under lubricated rolling-sliding contact fatigue.” Actual mating bodies and a FE model have explained in which a 2D half-space with an edge crack has an impact on a traveling contact load produced by a cylindrical body. Contrasts between this model and the different fluid pressurization methods have been made and the effects of the coplanar extension are analyzed. The outputs demonstrate that the fluid pressures within the crack generated by the fluid entrapment method will lead to the fluid pressurization method as the crack becomes short.

### **2.3 Fatigue Contact and Crack**

Fatigue cracks may begin at free surfaces or internal (subsurface) surfaces in the material, which is characteristic of metallurgical imperfections that create areas of higher stress. And from external flaws

such as scratches from poor treatment, machining deviation, surface roughness, or temperature deterioration (welding). When any material is subjected to fatigue, it causes progressive and localized structural damage. In this portion fatigue, contact, and its effect on crack are discussed

Y. Ding and J.A. Gear [50] investigated the Spalling depth forecasting model on a gear tooth. In this research, the growth of a gear spalling depth forecasting model is described. The spalling depths, determined by the model due to different contact loads and crack sizes, are compared with the practically estimated spalling depths generated under similar loading conditions. A good similarity between the forecasted spalling depth and experimental results is found.

B.L. Josephson et.al [51] elucidated the prediction of fatigue crack initiation for rolling contact fatigue. The Caboched material and finite element model for nonlinear isotropic and kinematic hardening were consumed. The ratcheting material response outcome was compared with an essential ratcheting model, and there was a safe concord regarding the per cycles to crack starting point and shear strain distribution below the contact surface.

K. Aslantas and S. Tasgetiren [52] studied the “modeling of spall formation in a plate made of Au tempered ductile iron having a subsurface-edge crack analysis of crack initiation and propagation under moving loads which is a complex phenomenon due to the non-uniform state of stress and singularity at the crack tip.” In this study, linear elastic fracture mechanics and finite element modeling predict spall formation in the elastic state. However, if materials move under power transmission, it is better to consider rolling-sliding contact fatigue in the materials.

M. Sraml and G. Fajdiga [53] proposed “fatigue crack initiation and propagation under cyclic contact loading”. The computational model for contact fatigue damage analysis of gear teeth flanks illustrated in detail. The model takes into account that the criteria required for the surface fatigue crack initiation and then permits for proper simulation of the fatigue crack propagation that guides to the presence of small pits on the contact surface. The crack theory and the finite element method have been utilized for the simulation of the fatigue crack growth. The virtual crack extension (VCE) method, implemented in the finite element method, is used for simulating the fatigue crack growth from the initial crack up to the formation of the surface pit. This research focuses on surface crack propagation under cyclic loading of gear flank. However, there is a rotational and somewhat translation motion of this flank that occurred during power transmission. So, consideration of rolling-sliding fatigue contact is very essential.

K. Aslantas and S. Tasgetiren[54] A study of spur gear pitting formation and life prediction. A numerical prediction of pitting formation in pitch gear made of ductile iron is made in this study. In this study. For the development of the analytical model, general two-dimensional sliding contact

situations are considered. Mixed-mode stress intensity factors  $K_I$  and  $K_{II}$  for cyclic loading are evaluated and related to crack extension by a Paris-type equation. The maximum tangential stress criterion is used to determine the crack-turn-angle during crack propagation under cyclic loading.

## 2.4 Surface crack

A crack can form on the surface of a substance. The primary cause of crack forming on any surface is fatigue and some defect (irregularity). We spoke about surface cracks and their properties in this post.

G. Fajdiga et.al [55] showed pitting formation in the contact of mechanical elements such as gears, bearings, wheels, etc. due to surface and sub-surface initiated fatigue crack growth. There is also a computer model for simulating the growth of fatigue crack caused by contact loading of both surfaces and surfaces. The model is based on the theory of fracture mechanics, where common fatigue tests achieve the required material properties. For computational simulations, instead of simulating the actual contact of mechanical elements, an equivalent model of two contact cylinders is used. The numerical results meet the available experimental data. The material properties needed to study crack growth propagation are very essential. So, the type of material on which the investigation is focus was not illustrated well.

A.V. Rychahivsky and Y. Kadin [7] proposed modeling of surface cracks in rolling contact. The authors used the finite element method for the simulation of the rolling of the cracked ball. By applying the linear elastic fracture mechanics approach, the crack criticality in terms of the stress intensity factors is identified. The parametric study regarding the levels of the contact load, crack shape, depth, and friction coefficient between crack's surfaces is presented. Here, in general, crack always does not stand from the surface of the materials but sub-surface of materials. So, studying the crack growth from the surface of the materials not that much important than that of the sub-surface. Because the crack always grows from the microstructure of the materials.

Amir Keidrich et.al [56] studied the propagation of surface-initiated rolling contact fatigue cracks in bearing steel. Most studies about rolling contact fatigue take full life into account. In contrast, the study studies the growth of rolling contact fatigue cracks to understand crack propagation mechanisms before they develop into surface pits. A three-contact disk machine was used for pitting experiments under closely controlled contact conditions in the mixed lubrication system on the bearing of steel samples. Experimentally tested crack propagation of surface pitting is demonstrated. However, sub-surface crack growth is not studied. Hence, crack always starts with the deterioration of the microstructure of the materials.

Kuhn Zhou and Rongbing Wei [57] studied Modeling cracks and inclusions near surfaces under contact loading. . For the multifaceted inclusions of the arbitrary shape beneath a half-space surface

that is subject to contact loading, a semi-analytical solution is developed. The quick algorithm of Fourier transform achieves computational efficiency. The solution is general and robust and may have extensive applications, in particular for wear and contact fatigue analyses, for reliability analysis on heterogeneous materials. The analysis is both in homogenous and heterogeneous materials but the effect is only considered on the surface of the materials but not on the subsurface.

## 2.5 Sub-Surface Crack

The distinction between a surface and a surface crack is the point of formation of the crack; a surface crack is on a crack, while a subsurface crack is on the subsurface. The effect of subsurface crack initiation and propagation is discussed in this section.

Dongfeng Zeng et.al [58] investigated the crack initiation of subsurface rolling contact fatigue in railway wheels. They used an experiment to investigate the crack initiation behavior, and then determine current forms and sizes of macroscopic faults in the wheel rim of the railway wheel RCF. The results of tests indicate that an ellipse can approximate the macroscopic defect. However, this study considers only the contact of rolling on the subsurface of railway wheels. But, not performed on through hardened materials.

Le Liu et.al [59] proposed a lifetime forecast for the propagation of sub-surface crack using a 3D dynamic FEA model and represents the spread of the subsurface crack to the gear system. In this research, the approach has been taken to remove stress intensities from Mode I and severely reduce stress intensities from Mode II in heavily loaded lubricated contacts by choosing the stress intensity factor. Through ANSYS Workbench transient analysis the accumulated plastically strain is selected to calculate the subfield splitting time from the 3-dimensional FEA model. Studying only propagation of the crack would not lead to a further conclusion on subsurface crack properties but, the size of crack propagation through different materials matters also. And rolling-sliding contact fatigue is also essential in crack propagation and nucleation however, it is not considered in the above author's work.

Nick Weinzapfel and Farshid Sadeghi [60] Proposed numerical modeling of spalling in rolling contacts initiated by sub-surface. The study mentioned the fact that the micro-structures topology had a 3D finite element model developed to study the stochastic nature of rolling tiredness. Material microstructure grains are modeled on random tessellations of Voronoi. Mechanics for continuous damage and partitioning of mesh are implemented to capture start and spread phases of fatigue damage which result in decay. Simulated fatigue breakdowns are similarly advanced to experimental observations of rolling contact fatigue. Here, only rolling contact fatigue of the materials and the FEM model are used to meet the experimental approach. However, the mechanical components always have to roll with invisible sliding contact so, considering rolling-sliding contact is very essential.

Arnab Ghosh et.al [61] demonstrated a fracture mechanics approach to Simulate Sub-surface Initiated Fretting Wear. In this investigation, a new approach based on shear stress reversal at the crack tips is implemented to propagate a subsurface-initiated crack under a fretting load. Hertzian line contact geometry is used to investigate the effects of different factors such as Hertzian pressure, coefficient of friction, displacement amplitude, and depth of the initial crack. Crack propagation paths and propagation life of the cracks under the surface are investigated in detail. The wear rates are also correlated to crack propagation rates and are in agreement with the dissipated energy wear coefficients obtained from the literature.

Sankaran Mahadevan et.al [62] Studies analysis of the propagation of the sub-surface crack in railway wheels using FEM rolling contact load. In this research, a general method is developed for analyzing the propagation of the subsurface crack for the problem of wheel/rail contact fatigue. And a technique of sub-modeling is also used for both computational efficiency and precision. Then a previously developed mixed-mode fatigue crack spread model will calculate the fatigue damage in the wheel. Afterward, the effects of wheel diameter, loading amplitude, initial crack size, location, and orientation on the stress intensity factor range were investigated using the proposed model. Finally, in-field observations are compared with the forecast results of the proposed methodology. The railroad wheels under motion were subjected to not only rolling contact but also sliding contact fatigue. However, the effect of sliding contact fatigue is not considered.

P. C. Bastias et al[63] investigated finite element modeling of subsurface cracks under contact loads. In this study, the Finite Element Model was introduced to simulate cracks in a double-dimensional rolling elastic half-space. For both a point load and a Hertzian pressure distribution, the mode II stress intensity range  $\Delta k_{II}$  is evaluated. The results concur with solutions in closed form. The model enables both long and short splits of any inclination to be studied. Although the model can be extended to treat friction and elastic-plastic behavior both by friction-less crack case and linear material behavior. The type of contact load applied in this research is only a 2D rolling contact load. Beyond 2D, considering more dimensional rolling-sliding contact is good for further research.

## **2.6 Numerical Analysis**

Computers' exponential growth has transformed research and practice in every science and engineering sector. Research and design approaches for delivering computerized solutions to science and engineering challenges are increasingly emerging for growing widespread use. For a long time, the finite element approach has been a fruitful research area. It is also becoming more popular as a research tool for numerical experiments. Dassault Systems sells Abaqus as part of their SIMULIA

Product Life-cycle Management (PLM) software tools as a suite of powerful engineering simulation programs based on the finite element method.

G. Fajdiga et.al [64] showed a simulation of the mathematical surface pitting because of loading contact. In this research, a two-dimensional mathematical model for simulating the pitching of mechanical elements is discussed. In the model, the initial break of 0.015 mm in the length of the contact surfaces is predictable because the material was previously processed thermally or mechanically. The numerical comparison with the available experimental results reveals that the proposed model effectively simulates the development of the surface fatigue crack under contact loading and can be used in computational surface frame prediction for various mechanical contact elements.

Mengyan Zang et.al [65] have examined reviews of the automotive laminated glass numerical impact failure analysis. The aim is to provide an overview of this auto laminated glass failure. Here are six numerical models to model the main damage pattern, the glass ply cracking process, followed by the implementation of plastic interlayer, PVB material models, which address three numerical adhesion modeling techniques introduced.

## **2.7 Summary**

Many researchers go through on both the surface and subsurface crack initiation and propagation of mechanical component failure under various parametric conditions were very important. Lubricant, inclination angle, friction coefficient, surface roughness, contact pressures, and other variables all have an impact on crack propagation. Even though many studies on computational methods for determining touch parametric effects have been conducted. This thesis work has the benefit of filling the gap of considering cracks induced at the subsurface studying the propagation of the crack under the effect of compressive mechanical load, friction and lubrication pressure effect using an efficient mathematical formulation found in ABAQUS known as extended finite element method.

## CHAPTER - 3 MATHEMATICAL MODELING AND METHODS

### 3.1 Materials

When stress is applied to the materials or mechanical components, it has to deform with a magnitude of strain that depends on the geometry of the body and its properties (such as modulus of elasticity, Poisson's ratio, and yield strength, hardness, and fracture toughness). In this paper, the contact mechanics model has been developed based on a 2D plane strain loading condition that is used to investigate crack initiation and propagation in the subsurface. The nucleation of cracks was predicted based on the comparison of resistance of martensite, mean (represents the mixture of martensite and austenite microstructure), and austenite materials with the contact stress distribution (in particular with the maximum shear stress). The material properties, such as yield strength of the materials can be determined from microhardness (HV0.1) tests [8], and the distribution of stress was analyzed based on the ring on ring loading configuration as illustrated using figure 3.1.

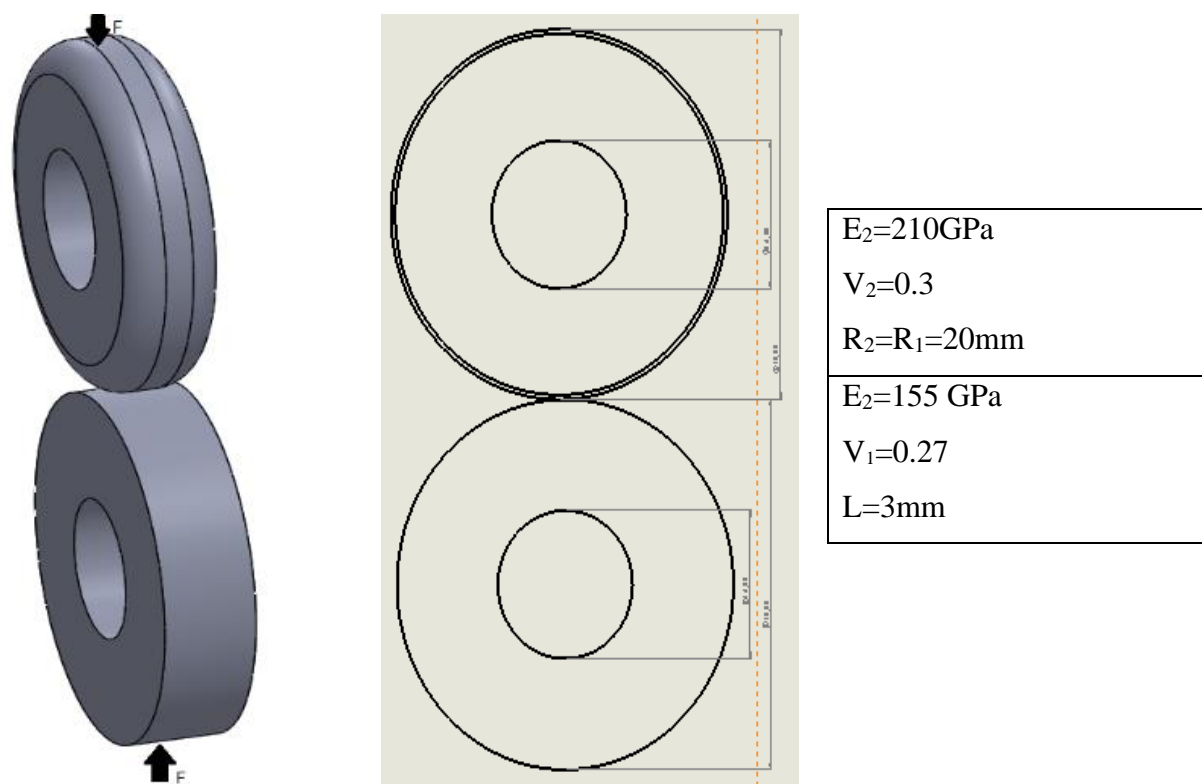


Figure 3. 1 schematically representation of the body

**Table 3. 1 Parameter of the material of the object [8]**

Property	Sintered through-hardened steel	Counter face disc
Density	7.0 g cm <sup>-3</sup>	7.25 g cm <sup>-3</sup>
Inner diameter	16 mm	16 mm
Outer diameter	40 mm	40 mm
height	10 mm	10 mm
furnace	1120 °C	1150 °C

The material properties mainly focus on this paper are Fracture toughness and yield stress. Fracture strength is a property that describes the ability of a crack-containing material to withstand further fracture and is an indication of the amount of stress required to spread the pre-existing fracture. This flaw may appear as cracks, voids, metallurgical inclusions, weld defects, or design discontinuities. Fracture strength is a quantitative way of expressing a material's resistance to fracture when cracking occurs. If the material has a high fracture strength, it is more likely to have a ductile fracture. Brittle fracture is characteristic of materials with less fracture toughness. Fracture toughness values may serve as a basis for:

- Material comparison
- Selection
- Structural flaw tolerance assessment
- Quality assurance

Stress intensity factor and plane strain fracture toughness factor, which has direct contact with materials fracture toughness. The stress-intensity factor (K) parameter is used to determine the fracture strength of most materials. The stress intensity factor is a function of loading, crack size and Structural geometry. K<sub>Ic</sub> is defined as the plane strain fracture toughness. It is a measure of the resistance of a material to crack extension under predominantly linear-elastic conditions. (i.e., low toughness conditions when there is little to no plastic deformation occurring at the crack tip) An approach is to perform a series of different experiments and reach a critical stress intensity factor K<sub>c</sub> for each material, this critical parameter when measured under certain conditions is known as the fracture toughness. The fracture toughness can be expressed as a function of the crack extension is called the resistance curve shows the Variation in fracture toughness with crack growth. Fracture toughness and material property values of materials and sintered steel types are listed below.

**Table 3. 2 Material property of slave disc object[8]**

Material	Density	Hardness (microhardness)	Yield strength (MPa)	Toughness ( $K_{IC}$ ) $MPa\sqrt{m}$	Elastic modulus (GPa)	Poisson ratio
Through hardened	$7.3^g/cm^3$	571	1333	36.74	155	0.27

#### Assumptions

- The crack can initiate at some depth from the surface of the sintered disc
- Mesh convergence is done for determining the contact stress only not for the crack analysis
- 2D plane strain condition

### 3.2 Mathematical Modeling of Subsurface crack

#### 3.2.1 Crack nucleation

In the common fracture mechanics representation, cracks are modeled as discontinuities possessing smooth and frictionless surfaces. A simple equivalent Hertzian contact model is used for simulating the fatigue crack propagation under given initial crack conditions of rolling and sliding contact. The contact model is subjected to only a normal compressive contact force. For the crack propagation simulation, the XFEM method in the framework of the FEM has been applied. It is assumed that the crack will propagate in the direction that maximizes the release of the strain energy, resulting in the minimum possible total potential energy of the system. This developed model has been used for the simulation of crack growth on two contact disc in-plane strain conditions. The property of the material for the master and slave disc is listed above and we assume that the coefficient of friction is zero. Then we calculate maximum pressure, average pressure the depth where crack us nucleate, critical fracture energy released. The presence of a very small defect and assume that a crack will initiate under the same conditions that would cause that flaw to propagate. The local stresses in the crack tip are analyzed according to the theory of elasticity in linear elastic fracture mechanics. Linear Elastic Fracture Mechanics considers three distinct modes of fracture: Modes I, II, and III.

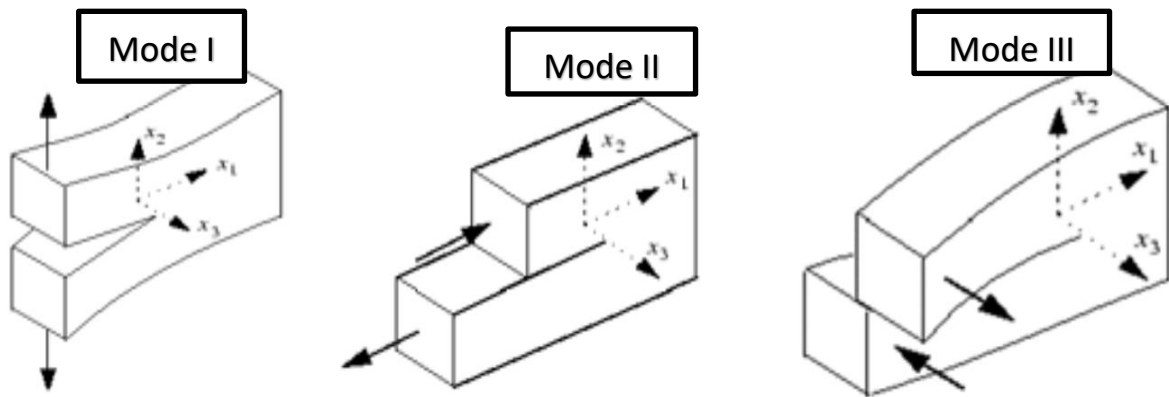


**Figure 3. 2 Modes of fracture**

- Mode I - opening mode when the tensile stress acting normal to the plane of the crack
- Mode II- sliding mode, this occurs when the shear stress is acting parallel to the plane of the crack and perpendicular to the crack front
- Mode II-tearing mode occurs when the shear stress acting parallel to the plane of the crack and parallel to the crack front

In subsurface crack propagation under rolling sliding contact, the object fracture mode is the sliding mode which means mode II.

So, first, we calculate critical fracture energy release.

$$G = \frac{K_{II}^2}{E'} \dots\dots\dots \text{Equation 3. 1}$$

$$E' = \frac{E}{1-\nu_1^2} \dots\dots\dots \text{Equation 3. 2}$$

$$G = K_{II}^2 \left( \frac{1-\nu_1^2}{E} \right) \dots\dots\dots \text{Equation 3. 3}$$

$$K_{II} = \tau x' y' \sin(\beta) \cos(\beta) \sqrt{\pi a} \dots\dots\dots \text{Equation 3. 4}$$

In mode II maximum  $K_{II}$  is at  $\beta = 45^\circ$

Fracture is initiated when:

$$K_I > K_{IC}$$

$K_{IC}$  is the material (intrinsic) property which characterizes the fracture behavior

And also crack extension occurs when  $G$  reaches the critical value  $G_C$

$$G > G_C$$

The critical energy release rate

$$G_c = K_{IC}^2 \left( \frac{1 - \nu_1^2}{E} \right)$$

$$G_c = (36.74 \text{ MPa}\sqrt{\text{m}})^2 \left( \frac{1 - 0.27^2}{155 \text{ MPa}} \right)$$

$$G_c = 8.074 \text{ N/mm}$$

The equivalent young's modulus of different property material is given below

$$E_c = \frac{E_1 E_2}{(1 - \nu_1^2) E_2 + (1 - \nu_2^2) E_1} \dots \dots \dots \text{Equation 3. 5}$$

$$E_c = \frac{210000 * 155000}{(1 - 0.3^2) 155000 + (1 - 0.27^2) 210000}$$

$$E_c = 96949.73 \text{ MPa}$$

The equivalent radial is

$$\frac{1}{R_c} = \frac{1}{R_1} + \frac{1}{R_2} \dots \dots \dots \text{Equation 3. 6}$$

$$R_c = \frac{R_1 R_2}{R_1 + R_2}$$

Half contact length

$$b = \sqrt{\frac{4R_c F}{\pi L E_c}} \dots \dots \dots \text{Equation 3. 7}$$

The maximum Hertzian pressure is

$$P_{max} = \frac{2F}{\pi b l} \dots \dots \dots \text{Equation 3. 8}$$

Average pressure is

$$P_o = 0.78 * P_{max} \dots \dots \dots \text{Equation 3. 9}$$

Where,

G - energy release rate to create a crack surface or it is the net change of potential energy that accompanies the increment of crack extension

G<sub>c</sub> -critical energy release rate

K<sub>II</sub> - stress intensity factor at mode II opening crack (stress)

K<sub>IC</sub> - critical value of stress intensity factor which is also called fracture toughness

τ<sub>x'y'</sub>- Shear stress

β - Crack inclination angle

a - Crack length

$\sigma_{\max}$  = Maximum Hertzian Stress

$l$  = Contact length, mm

$F$  = Applied force, N

$P_{\max}$  = Maximum Hertzian Pressure, MPa

$b$  = Half Contact Width, mm

$R_c$  = Equivalent contact radius, mm

$E_c$  = Equivalent Elastic moduli, MPa

$E$  = Elastic modulus of contacting elements, MPa

$\nu$  = Poisson's ratio

### 3.3 Finite element modeling of contact mechanics and crack propagations

The Finite Element Method (FEM) is the most commonly used method to solve engineering problems. It is an accurate numerical method for solving partial differential equations in several variables. To solve a problem, the FEM divides a large system into smaller, simpler parts called finite elements. The Finite Element Analysis (FEA) is a simulation of any given physical phenomenon using a numerical technique called the Finite Element Method (FEM). Engineers use it to reduce the number of physical prototypes and experiments and to optimize components in their design phase to develop better products, faster and cost-saving. Mathematics must be used to fully understand and quantify any physical phenomena such as structural or fluid behavior, thermal transport, wave propagation, growth of biological cells, etc. Most of these processes are described using partial differential equations (PDEs). However, for a computer to solve these PDEs, numerical techniques have been developed over the last few decades, and one of the most important is the Finite Element Analysis.

#### 3.3.1 Method of fracture mechanics analysis

There are two ways to analyze the mechanism of crack initiation and propagation, these are

- ◆ Based on fracture mechanics- damage is modeled as one or more than one sharp crack in the structure crack initiation and propagation is the analysis
- ◆ Based on continuum mechanics-there will be no initiation or propagation of a sharp crack in the structure. damage is initiated and propagated through downgrading elements and element removal

In this paper, we use the fracture mechanism method to analyze crack initiation and propagation. After knowing the mechanism, we must identify the criteria of evaluation, to evaluate crack propagation in fracture mechanism there are some ways of setting the criteria for evolution, which are

- Energy criteria
- Displacement criteria

In this paper, the energy criteria are used which shows when the fracture energy of the material less than the energy release rate and then only propagated but we should find the optimal mesh size with convergence analysis which has a Greater influence on crack propagation. Finally, we select the appropriate technique of analysis to solve our problem there are some techniques

- Contour integral is a traditional technique for analyzing stationary cracks (the crack we assume does not propagate). By using this technique, you can calculate the stress intensity factor (SIF), J-integral, CT-integral, and T-stress in a static or quasi-static problem. This technique cannot simulate the crack initiation and crack propagation and only available abacuses/standard solver
- XFEM (extended finite element method)-it can analyze stationary cracks like contour integral techniques only in 3D space because XFEM cracks cannot be stationary in 2D space. Simulate cracks initiation and crack propagation in the static, que-static, and dynamic problems. The calculation will be solution-dependent and the algorism will calculate the crack propagation direction automatically and without any limitation.it used for simulating crack propagation in both the ductile and brittle material. This technique is only available in abacus/standard solver
- CZM (cohesive zone method) - uses in both cohesive elements and cohesive surface.it can be used for modeling delamination and damage propagation in adhesive connections and connection with cohesive behavior. This technique is available in both abacus /standard and Abaqus/explicit.it can use for modeling static, qua-static, and dynamic problems.
- VCCT (virtual crack closure technique) we can use VCCT to study a crack in parts containing geometry, orphan mesh elements, or a combination of the two and can define a VCCT crack in the Interaction module. It can specify the location of the surfaces that are initially bonded. VCCT is available only for Abaqus/Standard (three-dimensional solid, shell, and two-dimensional planar and axisymmetric models).

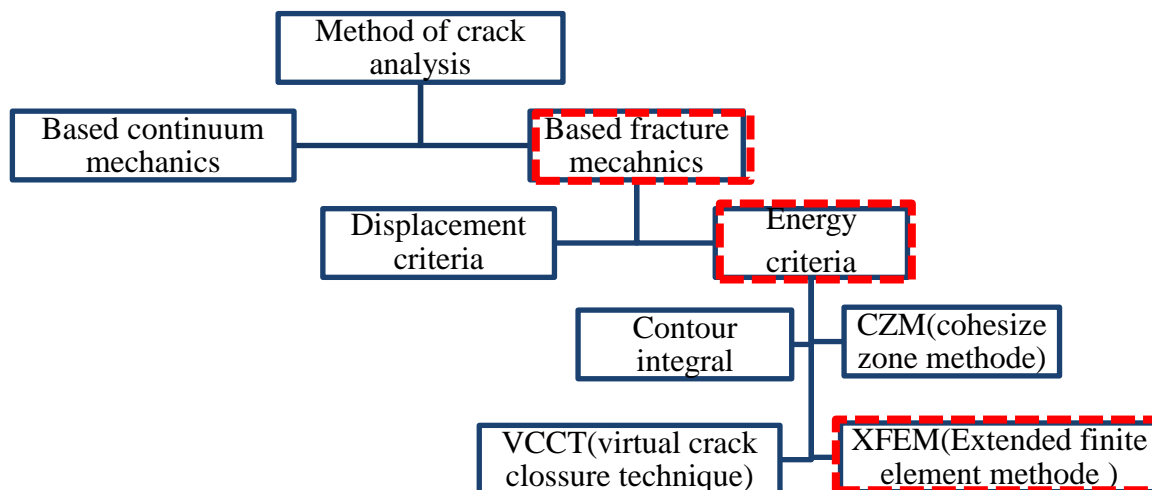


**Figure 3. 3 Methods crack analysis**

Therefore, the suitable technique for this paper is the extended finite element method (XFEM). Therefore, in this paper subsurface crack propagation are solve by fracture mechanism by using energy criteria and used XFEM technique.

### 3.3.1 Unit systems in ABAQUS

Abaqus does not identify a unit system; the operator could use a unit system randomly, as long as they are in uniformity in the analysis problem made[14]. The operator uses constant basic units in Abaqus.

**Table 3. 3 System unit in Abaqus**

Parameter	Units
Force/load	Newton (N)
Displacement	millimeter (mm)
Mass	Tone (10 <sup>3</sup> kilograms)
Time	Second (S)
Stress	MPa (N/mm <sup>2</sup> )
Energy	MJ (10 <sup>-3</sup> )
Density	Tone/mm <sup>3</sup>

### 3.4 Numerical modeling of contacting elements using Abaqus

#### 3.4.1 Crate Part

We use a two-dimensional model Extended Finite element analysis has many steps to analyze structures. The first thing is to understand the program and the problem occurs object. In understanding the object, we can identify the element type. It can be shell, solid, or wire elements. The shell type can take the form of a linear or quadratic shape. The development of the model has several steps. The first step is the drawing of the part using ABAQUS software. There is a drawing feature Part section is used to draw the geometry of the object, which makes it possible to draw the parts. The parts are planner deformable shell base. The next one is the simulation; it is carried out under isotropic material for both the master disc and slave disc with linear elastic fracture mechanics.

**Table 3. 4 Dimensions of master and slave disc**

Part name	Modeling space	type	Feature shape	Feature type	Outer diameter	Inner diameter
Mater disc	2D	Deformable	Solid	planner	40	20
Slave disc	2D	Deformable	Solid	planner	40	20

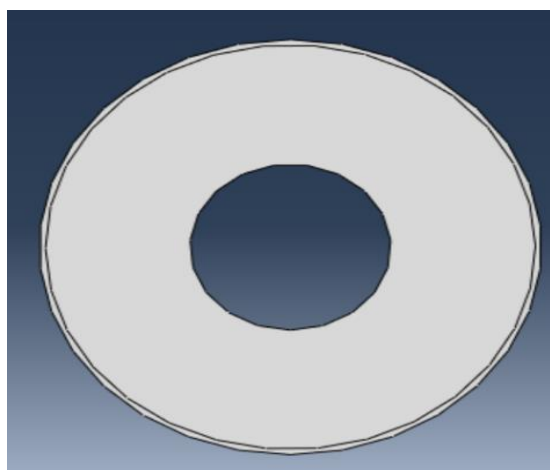


**Figure 3. 4 master disc modeling**



**Figure 3. 5 slave disc modeling**

#### 3.4.2 Material Property Section

In the property section, material properties and body sections are assigned to specified regions of the master and slave disc. The master disc and slave disc have the same material behavior, type, and section.

**Table 3. 5 Material property of master and slave disc[8]**

Part name	Material behavior	type	Young modules	Poisson's ratio	Section type
Master disc	elastic	isotropic	210000MPa	0.3	Solid, homogenous
Slave disc	elastic	isotropic	155000MPa	0.27	Solid, homogenous

### 3.4.3 Assembly Section

This section shows the development of basic contact modeling using Abaqus for creating the instances of parts. The object has one assembly, that composed of master and slave disc and they are assembled in this section.

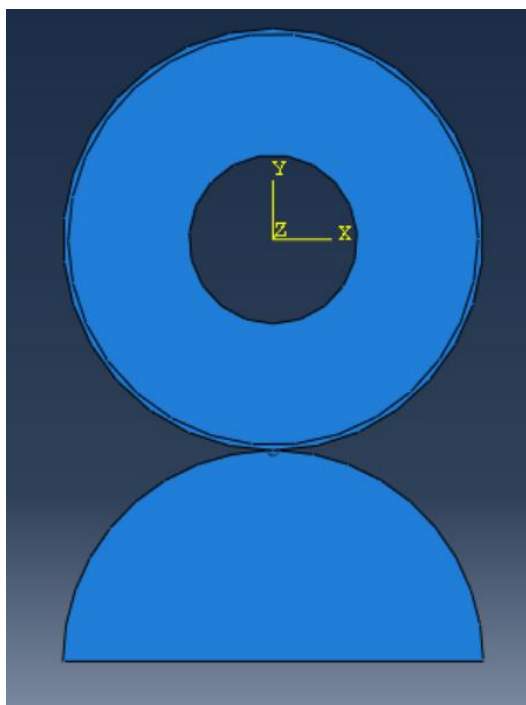


**Figure 3. 6 Assembly model of master and slave disc**

### 3.4.4 Step Section

The step section creates a different type of steps for analyzing and useful to make single steps for each change in the model. Every step can recommend what the output parameters have to be. Also, the length of the step, the actual simulation time can be set. As well as the start, the minimum and maximum value of a single increment, and the maximum number of increments. In the initial step, the

model is checked correctly and the output requests are demanded each step is possible. In the first step, the force is applied at the center point of the hollow master disc. In the second step, this force is conserved and the disc starts to rotate with a given speed.

**Table 3. 6 Static model analysis parameters**

Step	Step name	Procedure	Period	Increment size			Maximum increment
				Initial	Minimum	Maximum	
0	Initial	Initial	N/A	N/A	N/A	N/A	N/A
1	Applying force	Static general	1	0.1	0.005	1	100
2	Rotational	Static general	1	0.1	0.0005	1	100

#### 3.4.4.1 Creating amplitude

**Table 3. 7 Tabular presentations of amplitude through the steps**

Name	Type	Time spam	Smoothing	Amplitude data	
				Time/frequency	Amplitude
Rotation amp	Tabular	Step time	Use solver default	0	0
				1	1
Load amp	Tabular	Total time	Use solver default	0	1
				1	1
				2	1

#### 3.4.5 Interaction Section

In this section, we select the type of contact, which is held in two objects; Surface-to-surface contact interactions describe contact between two surfaces. The penalty of friction was included in the contact pair to define the friction behavior of the contact region. Besides, can define contact between edges of wire or between faces of a solid or shell. Certain connectivity restrictions apply to contact surfaces depending on the type of contact formulation.

**Table 3. 8 Contact type and property**

Interacting part	Interaction type	Contact property	Normal behavior	Contact formulation
Master with slave disc	Surface to surface	Tangential behavior	Hard/soft contact	frictionless

### 3.4.6 Boundary Condition and load Application

In the case of a two-disc machine, the apparent contact area is elliptical. And, the two disks rotate at the velocity  $V_1$  and  $V_2$ , where  $V_1 \neq V_2$ . The existence of a slip between the two disks, together with the normal load acting on them, results in sliding wear. Such a system is similar to that one shown on the right-hand side, in which the bottom disk is fixed and the top disk rotates. The Slide speed  $V = |V_1 - V_2|$ . With this assumption, the problem may be reduced from a rolling sliding contact to a sliding contact.

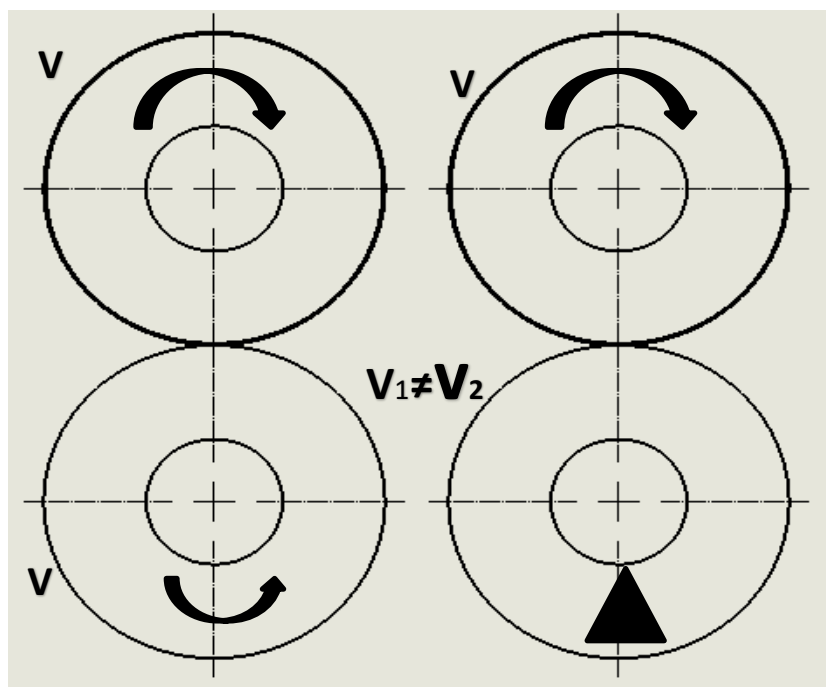


**Figure 3. 7 Mode of simplification rolling sliding contact to sliding contact**

So, after finalizing the interaction section, we came to the load section. In this section, we define the loads and boundary conditions of the objects. The concentrated forces are applied to the model in the Y direction at the center of the master disc. In the next boundary condition, to simulate the master-

slave simulation the BC's must be selected properly. Therefore, the center node movements in the X stand Y direction are blocked and rotations around the Z-axis vector are free as well and the simplified slave disc is fixed at the bottom in all directions.

**Table 3. 9 Boundaries and load condition**

Name	Load	BC-1	BC-2
Type	Concentrated force	Displacement/rotation	Symmetric/Antisymmetric/encastre
Step	Step-1 (static general)	Step-2 (static general)	Initial
Region	Set-7	Set-10	Set-11
Distribution	Uniform	Uniform	-
Location	At the center of the master disc	At the outer surface of the master disc	At the lower edge of the slave disc
Magnitude	650 MPa	4.2	zero
Direction	Negative y-direction	UR3	All direction
Amplitude	Load -amp	Rotation-amp	-

### 3.4.7 Meshing

The finite element mesh is generated by selecting the meshing technique that ABAQUS uses to create the mesh, the element shape, and the element type with the different number of meshing techniques for the best consistent mesh refinement by seeding the edge of the part to the appropriate element size.

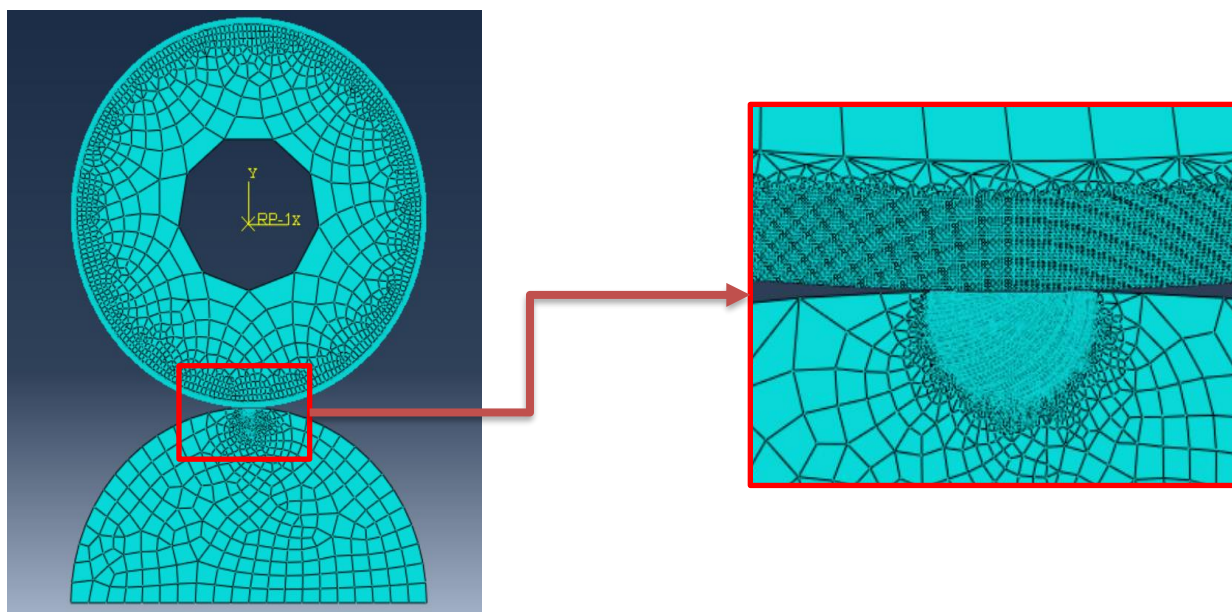


**Figure 3. 8 The finite element mesh of the object**

### 3.4.7.1 Mesh optimization analysis

Different solutions can be adopted while meshing a master and slave disc for equivalent stress. The mesh size at the contact interface should be fine to capture the relaxed stress state near the contact, between the master and slave disc surface. To do a mesh convergence study to find a mesh size that produces correct results, the modeling with mesh refinement was continued until an appropriate convergence of the stress state was achieved without using too many elements which increase calculation time. The study uses maximum von-misses stress and is set up with an average element size from 1mm to 0.01 mm. Various arrangements can be embraced while coinciding with an ace slave plate for identical pressure. The work size at the contact interface should be fine to catch the casual pressure state close to the contact between the ace and slave circle surface.

**Table 3. 10 Parameters of mesh convergency**

Mesh type	Local mesh element size	Number of elements	Numerical equivalent stress	Hertzian equivalent stress
1	0.001	235897	397.3 MPa	398 MPa
2	0.01	199875	396 MPa	398 MPa
3	0.02	177529	390 MPa	398 MPa
4	0.04	49047	286 MPa	398 MPa
5	0.06	22078	238 MPa	398 MPa
6	0.08	13587	106 MPa	398 MPa
7	0.1	10960	98 MPa	398 MPa

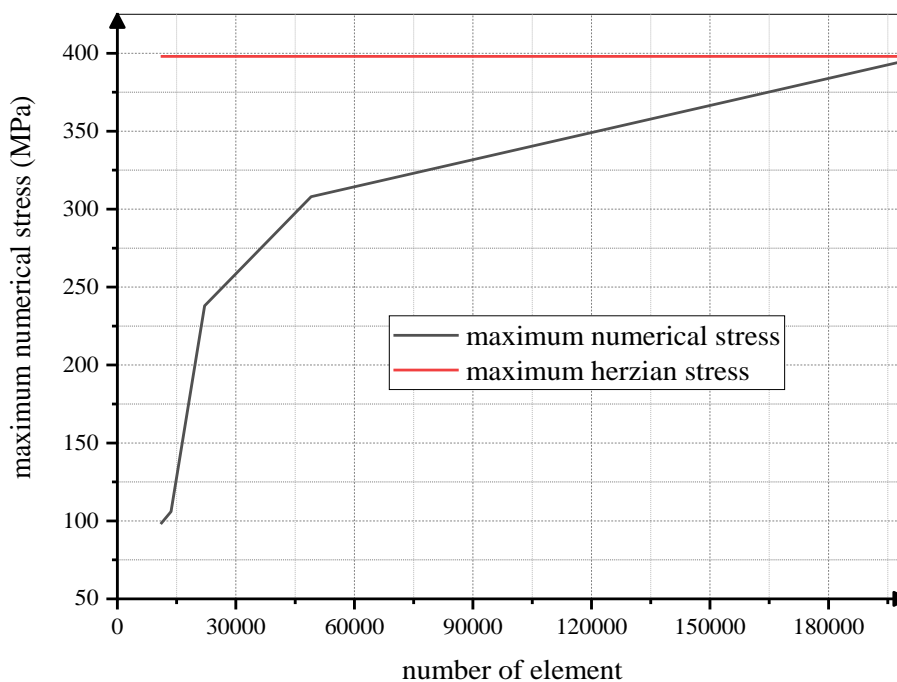


**Figure 3. 9 Mesh convergence analysis**

According to mesh convergence study results, an acceptable element size was determined to be at least less than 0.001mm in the refined contact zone.

**Table 3. 11 Mesh property of master and slave disc**

Types of disc	Element type	Element library	Geometric order	Family	Element size
Mater disc	CPE4R	Standard	Linear	Plain strain	0.005
Slav disc	CPE4R	Standard	Linear	Plain strain	0.001

### 3.4.8 Job, Simulation and Post-Processing

After finishing, all of the steps in defining a model and then using the Job section to analyze the model. First creating a job, submit it for analysis, and observe its progress. And in the visualizing section, the output requested in terms of the graphical display of the finite element model and result in Plot Contours on the deformed and undeformed shape, contours, graphs, animations of analysis with respective visualization variable value and animation scale factor.

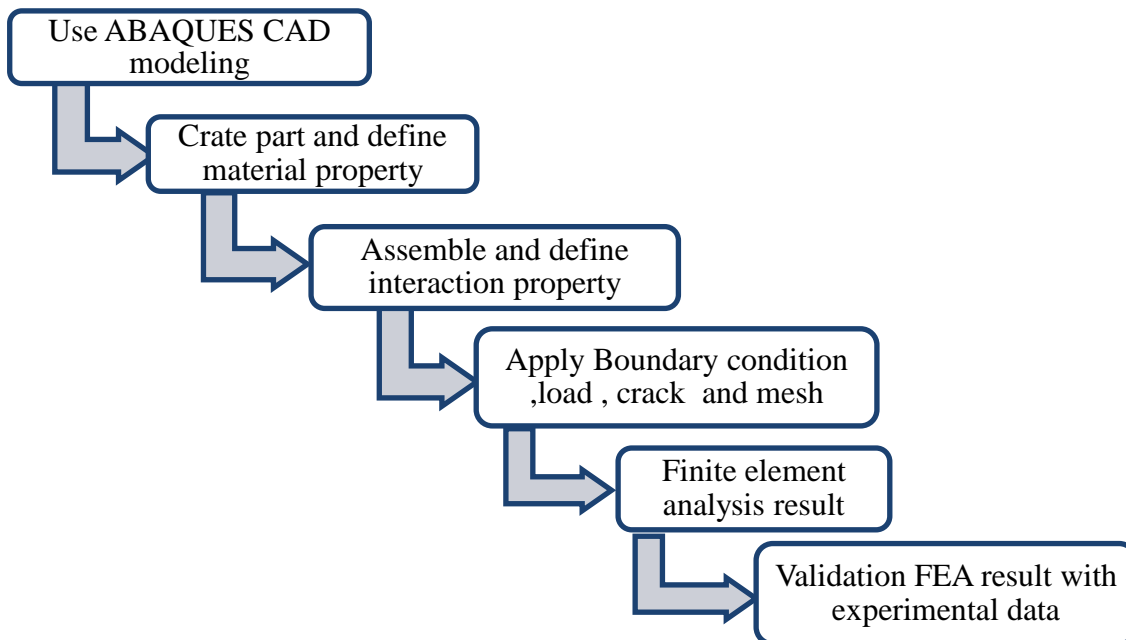


**Figure 3. 10 Summary of numerical analysis**

## CHAPTER - 4 RESULT AND DISCUSSION

In this chapter, the selected study methods described in Chapter 3 with their experimental counterparts are used. Other researchers' experimental tests are used for comparison. This chapter discusses the method's prediction results for the selected model.

### 4.1 The effect of load on the stress distribution

To find the effect of applied load on the shear stress distribution and depth  $z$  (where shear stress is maximum). In this topic paper, the effect of load on stress distribution the location or position where the maximum shear stress appears is analyzed. Table 4.1 presents the effect of the applying load on maximum shear stress existing point.

**Table 4. 1**The effect of load on the depth of maximum shear stress exists

Applied Load (N)	Maximum shear stress (MPa)	Depth of maximum shear stress (Z)(mm)	Half contact width (b)(mm)
295	550	0.033	0.11
376	622	0.039	0.13
475	700	0.044	0.14

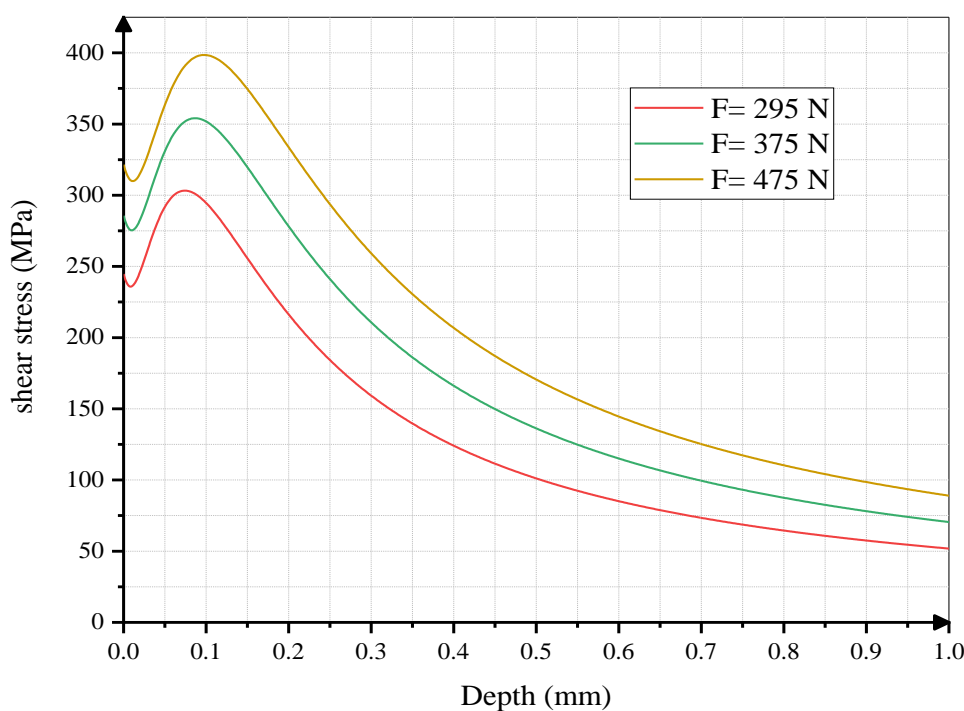


**Figure 4. 1** The effect of load on the distribution and depth of maximum shear stress exists

Therefore, when the applied load is increasing the depth of maximum shear stress appears is also increase or being far from the surface. Moreover, the maximum shear stress is an increase in the condition when the load is increased.

#### 4.2 The effect of contact surface friction on stress distribution

The influence of the coefficient of contact friction ( $\mu$ ) on the maximum equivalent stress distribution on rolling sliding disc mechanical elements is evaluated numerically using Abaqus CAE and Abaqus standard. Figure 4.2 represents the effect of the surface friction coefficient on the maximum equivalent stress in the materials without considering the initial crack.

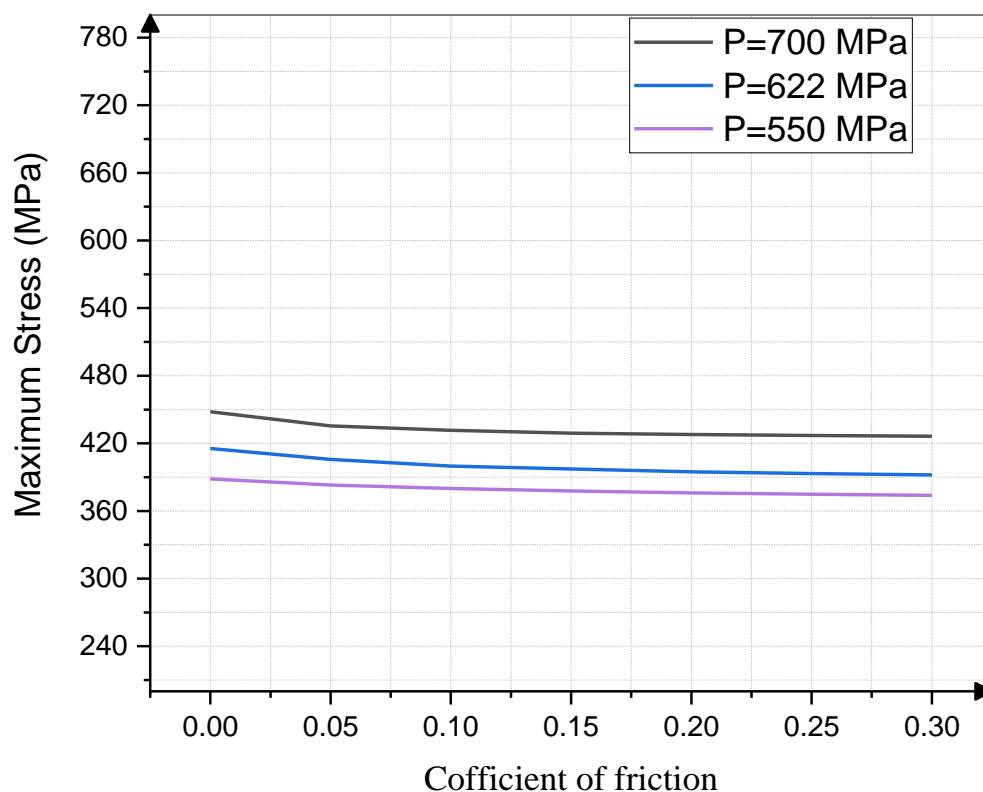


**Figure 4. 2 Shear stress distribution with different coefficient of friction without initial crack**

The results of coefficient of friction versus maximum equivalent stress show that maximum stress is not affected significantly by the variation of coefficient of friction and fixed loading conditions. However, linear variation was observed as the initial crack face is introduced in the analysis. Figure 4.3 represents the maximum equivalent stress near the crack tip by varying the surface friction coefficient.

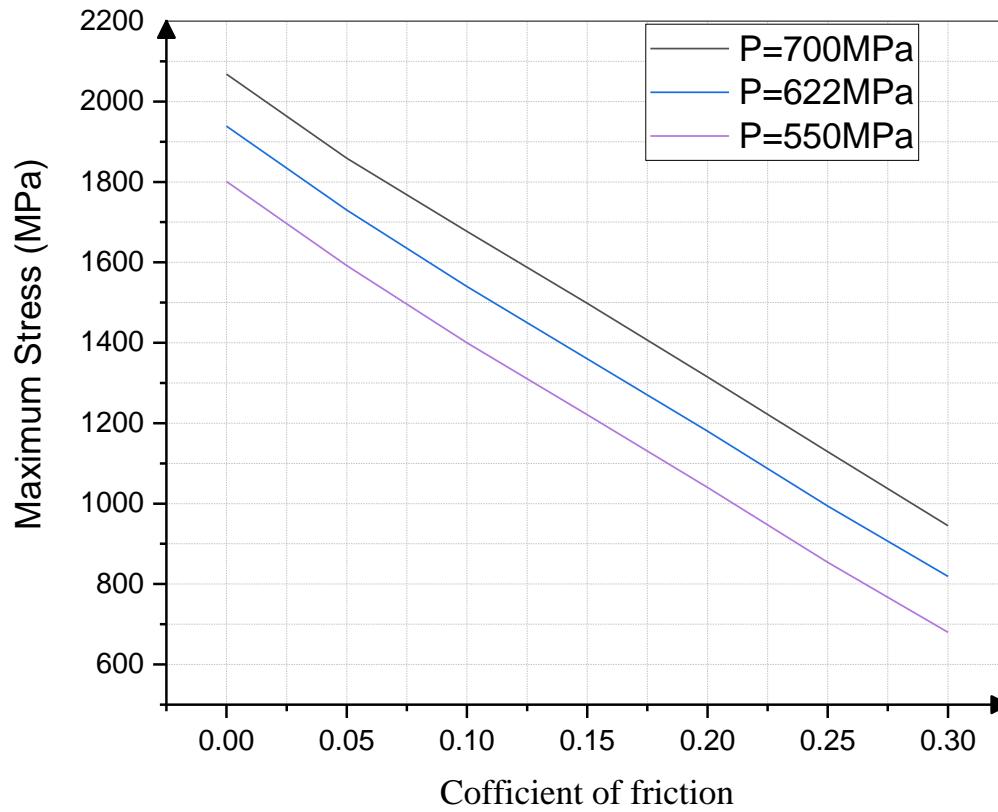


**Figure 4. 3 Shear stress distribution with different coefficient of friction with initial crack**

Since the position of the maximum equivalent stress goes to the surface as the coefficient of friction increases from 0 to 0.3, the intensified equivalent stress near the crack tip decreases with the increased coefficient of friction. Also, the distribution of equivalent stress was present in the form of contour using figure 4.4.

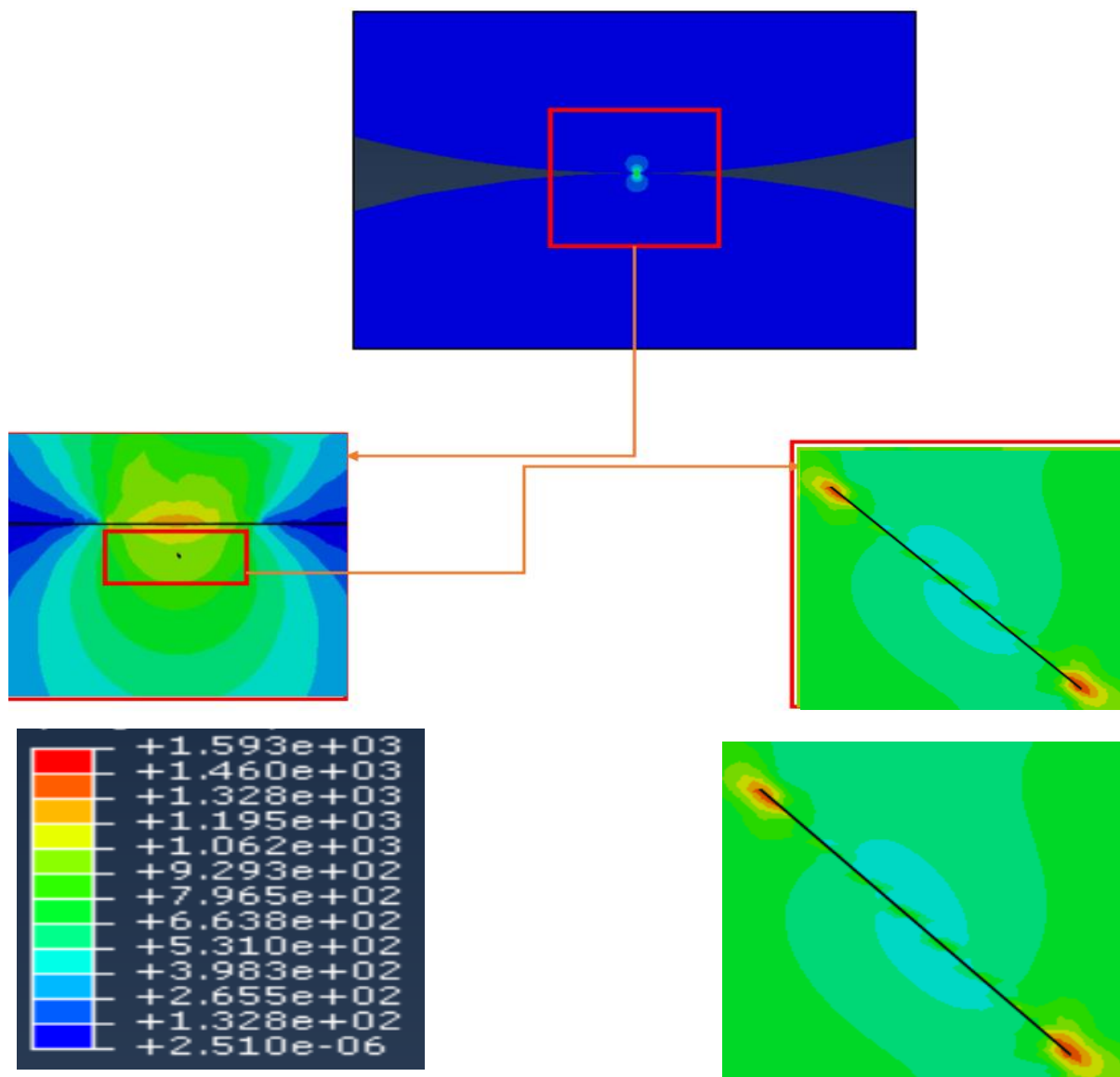


**Figure 4. 4 Contour map of equivalent stress distribution at the 622 MPa pressure and 0.17 coefficient of friction.**

The Simulations showed that for different values of friction  $\mu$  the influence on the shear stresses in the depth of contact area. With decreasing the coefficient of friction decrease the shear stress and goes far from the surface to the maximum depth of ( $Z=0.63b$ ) starting at a friction coefficient is zero and so with increase the coefficient of friction the maximum shear stress decrease and there is no change of position of maximum shear exist because maximum shear always exists on the crack tip.

### 4.3 The effect of crack angle on the stress distribution

This part of the paper investigates the effect of crack angle on stress distribution propagation. Figure 4.5 represents the maximum equivalent stress with variable crack angles

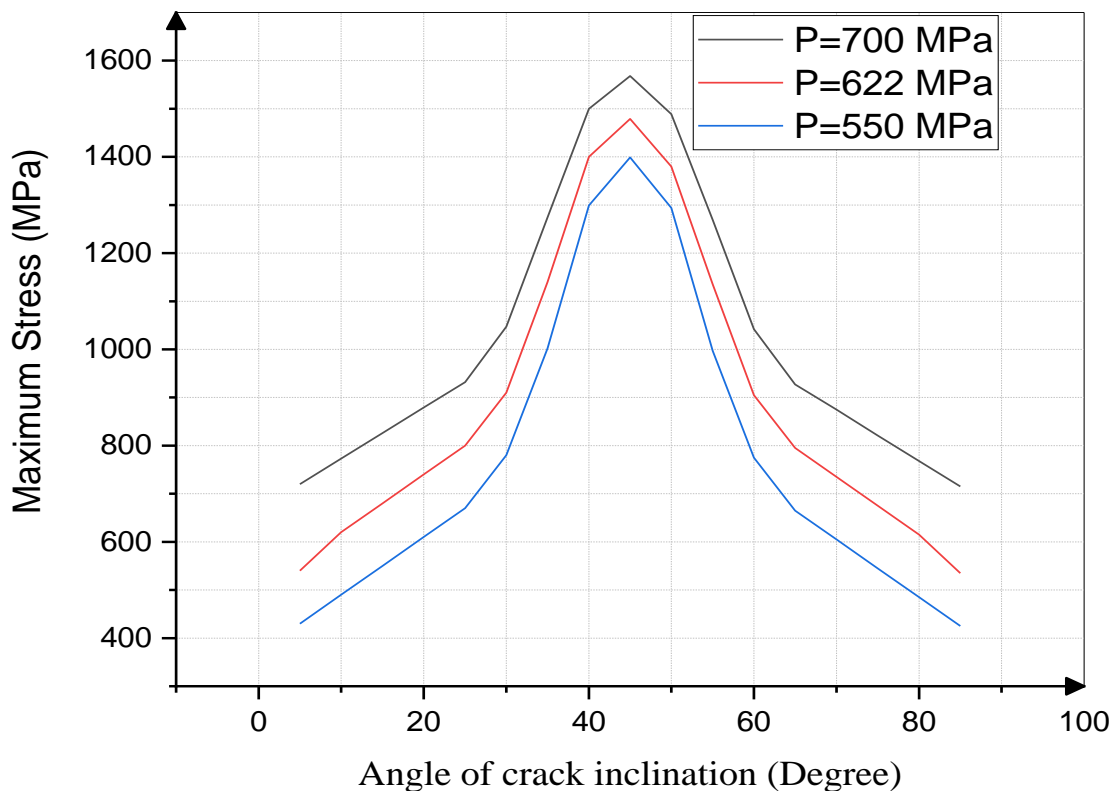


**Figure 4. 5 Shear stress distribution with different Crack Angle**

The maximum equivalent stress is observed when the crack inclination is about 45 degrees. As the crack orientation concedes with the shear plane (where the principal contact shear stress exists, which is the cause of crack nucleation and propagation of materials subjected to contact load), equivalent stress becomes maximum. Therefore, the shear plane is the critical crack direction that could affect strongly the crack propagation

#### **4.4 Crack propagation**

In this section the following results are presented and discussed;

- A. the effect of applied load on the crack propagation
- B. the effect of surface friction of the crack propagation
- C. the effect of crack angle on the crack propagation

##### **A. The effect of applied load on propagated crack length**

The effect of applied load on propagated crack length is evaluated using FEM with the tool of Abaqus CAE. The effect of applied load on propagated crack length is shown in Figure 4.6.

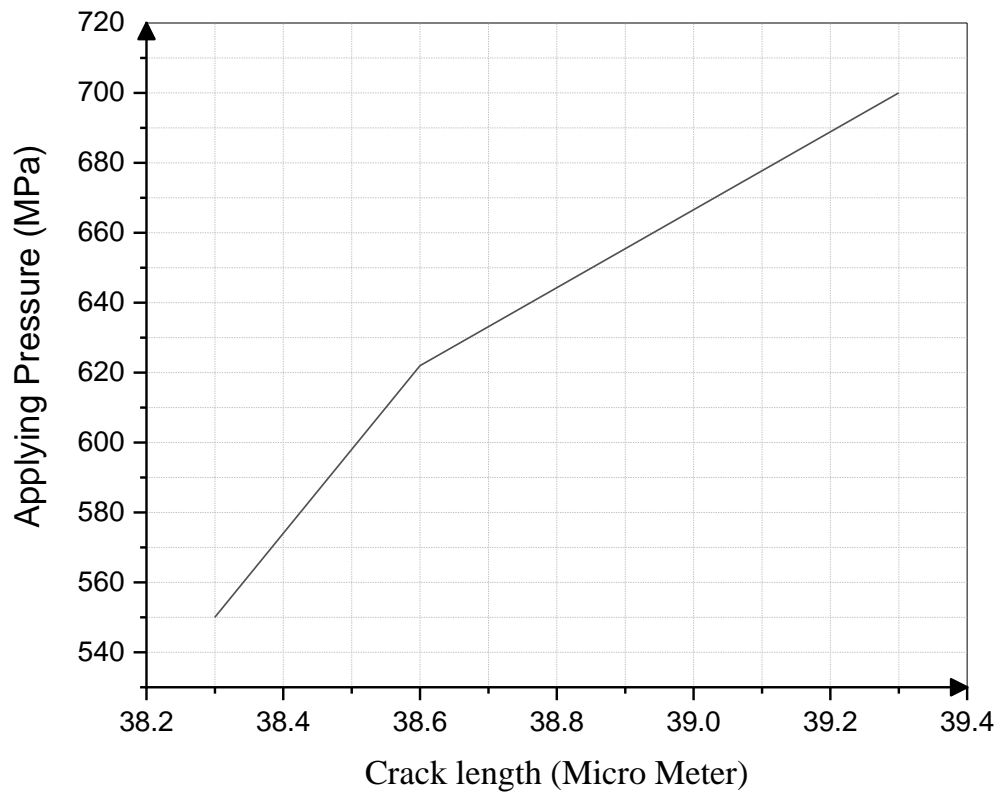


**Figure 4. 6 crack length and the influence of applying pressure**

The crack grows with two different stages as the load increases from 550 MPa to 700 MPa mean pressures. In the first stage, as load increases from 550 MPa to 620 MPa mean pressures, the propagated crack length increases linearly, and in the second stage as the load increases further the crack grows linearly which shows relatively lower slope as compared with the first stage of crack growth. The transition from the first to the second stage may relate to the variation of the position or depth of maximum equivalent stress (as presented in figure 4.1) at different applied loads. Figure 4.7 represents the contour of maximum stress distribution around the crack tip (initial crack is inserted at the position of maximum equivalent stress of 622 MPa applied mean pressure) at 550 MPa, 622 MPa, and 700 MPa.

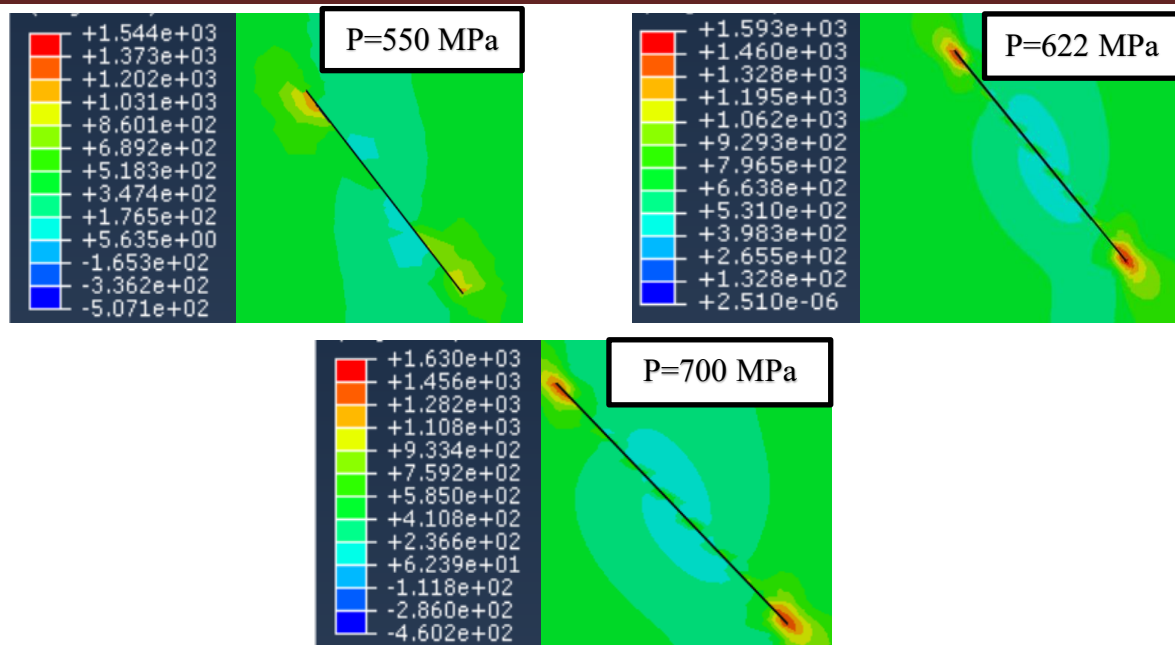


Figure 4. 7 The contour map of maximum stress distribution around the crack tip

### B. The effect of surface friction on the crack propagation

The effect of the coefficient of surface contact friction ( $\mu$ ) on crack propagation is numerically investigated. Figure 4.8 represents the effect of the surface friction coefficient on the crack propagation length.

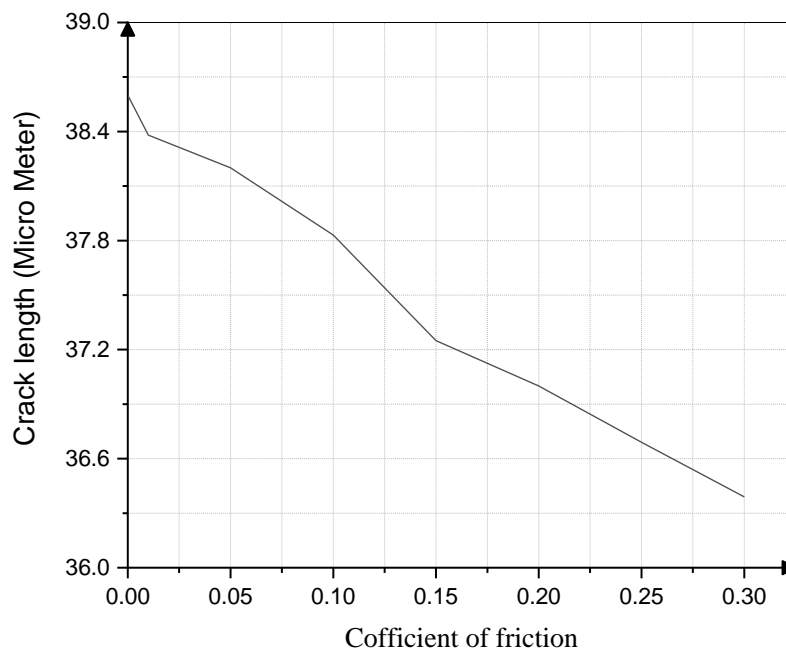
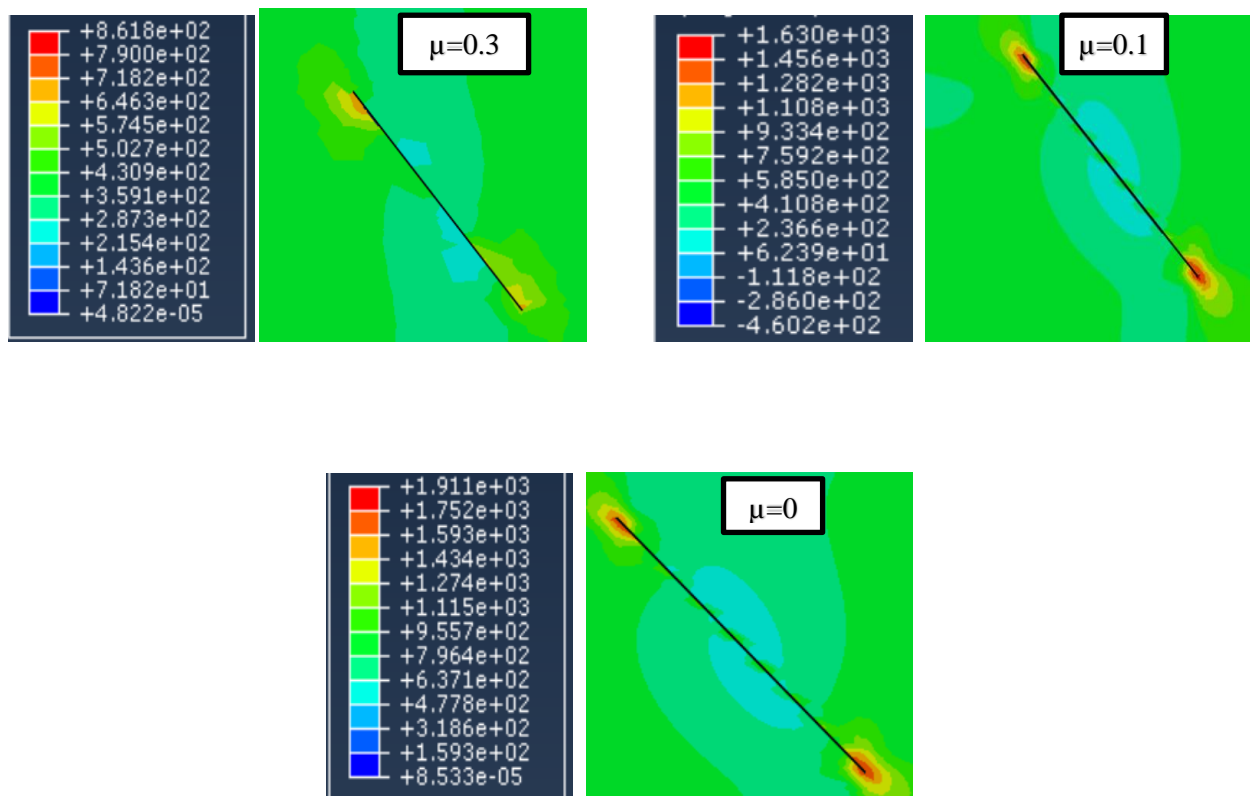


Figure 4. 8 the effect of surface friction of the crack propagation

The results show that the coefficient of surface friction has a major impact on propagated crack length. As the coefficient of friction decreases from 0.3 to 0, the crack length increase. The decrement of the subsurface crack length is related to the shift of maximum equivalent stress position towards the surface as the coefficient of friction increases. The effect of coefficient of friction on the depth of maximum equivalent stress is illustrated using figure 4.9; the three equivalent stress distributions of the counties are prepared by applying a load of 622 MPa mean pressure and for the coefficient of friction of 0, 0.1, and 0.3.



**Figure 4. 9** The contour map of equivalent stress distributions prepared by applying a load of 622 MPa pressure and for the coefficient of friction of 0, 0.1, and 0.3.

### C. The effect of crack angle on crack propagation

Using Abaqus CAE and Abaqus standard, the effect of crack angle on crack propagation is numerically evaluated. Figure 4.10 described the maximum crack length with variable crack angles

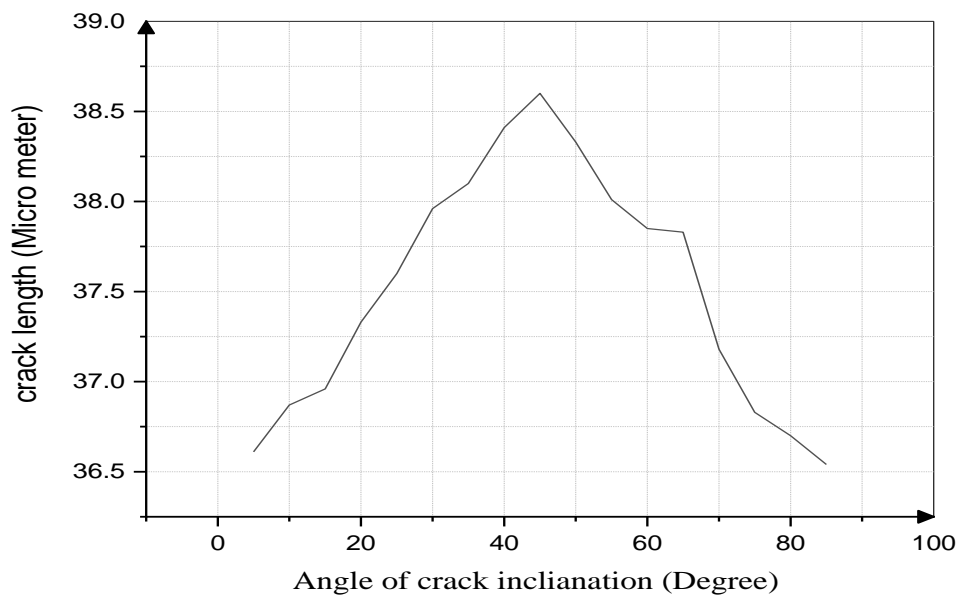


**Figure 4. 10 The effect of crack angle on the crack propagation**

Figure 4.11 presents the three equivalent stress distributions of the counties are prepared by applying a load of 622 MPa mean pressure and angle of crack inclination  $\theta= 25^\circ, 45^\circ,$  and  $75^\circ$ .

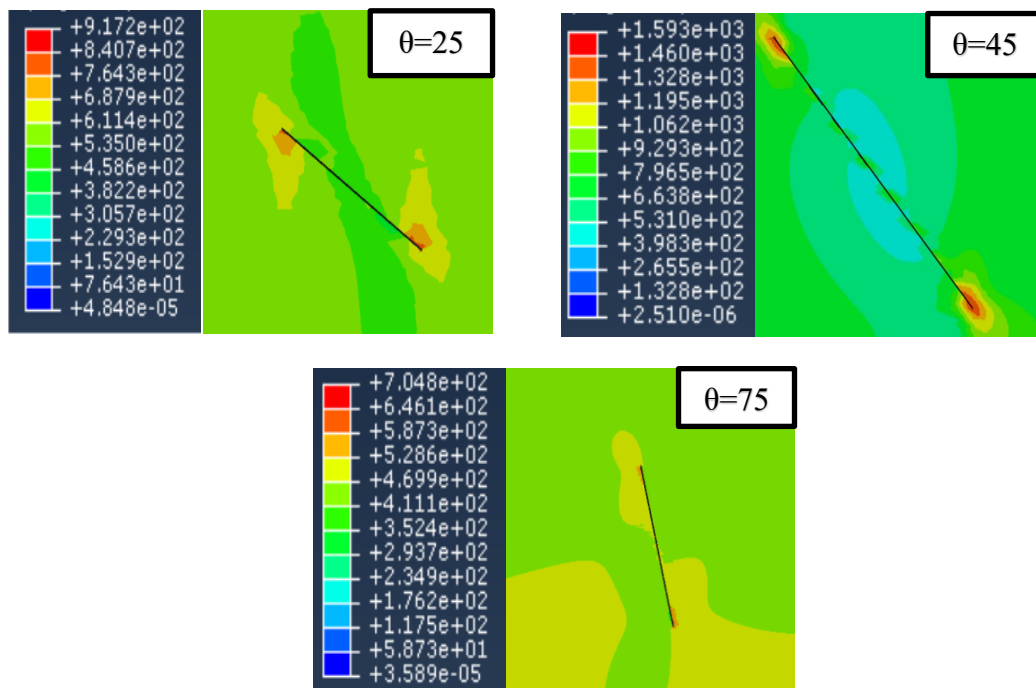


**Figure 4. 11 The contour map of equivalent stress distributions prepared by applying a load of 622 MPa pressure and for the crack**

When the crack inclination is about 45 degrees, the maximum crack length is observed. Crack propagation through-hardened steel subjected under rolling-sliding contact was studied using the finite element method at a maximum applied load (622 MPa) and 0.17 coefficient of friction. The nucleated surface crack is observed at this pressure and 45-degree of inclination as it was observed by the experimental study, the initial length of the crack is 10  $\mu\text{m}$  then after applying the load it propagated to 37.973  $\mu\text{m}$ .

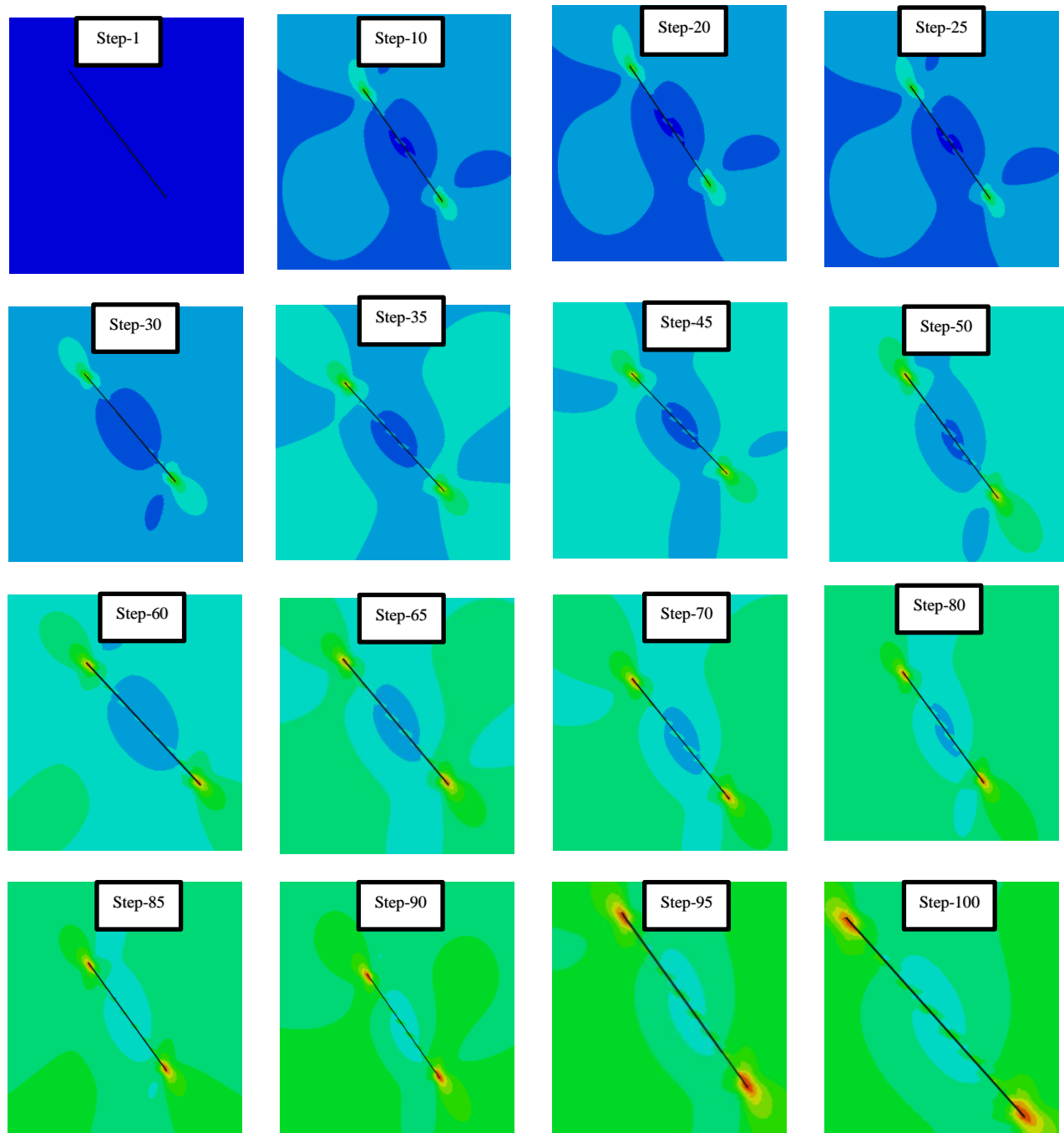


Figure 4. 12 The output of crack propagation with increasing cyclic load

According to the numerical results, XFEM the crack propagates in mode II at a pressure of 622MPa. The crack propagates where the numerical fracture energy release rate greater than material fracture toughness. The above figure, Figure 4.12 represents the crack propagation at different cyclic steps by applying only 622 MPa and 0.17 contact surface frictions.

#### 4.5 Validation using the experimental results

In this sub-section, the results of the numerical (ABAQUS) analysis and the experimental analysis for Subsurface crack propagation in through-hardened steel subjected under rolling -sliding contact are presented. Figure 4. 12 represents the analytical prediction of crack nucleation and the experimental results (nucleated crack and propagated cracks).

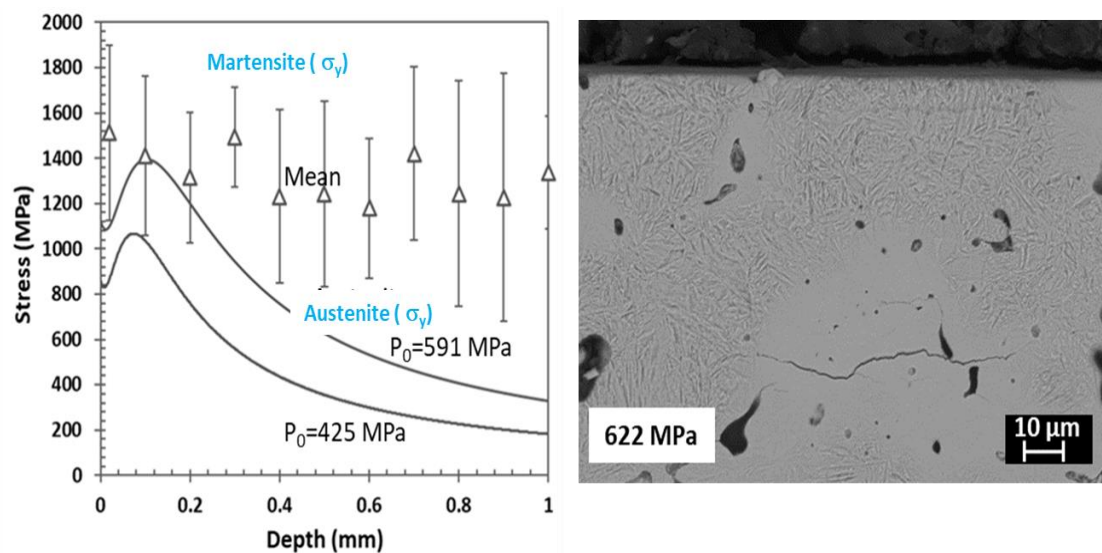


Figure 4. 13 mean pressure and crack initiation of experimental data[8]

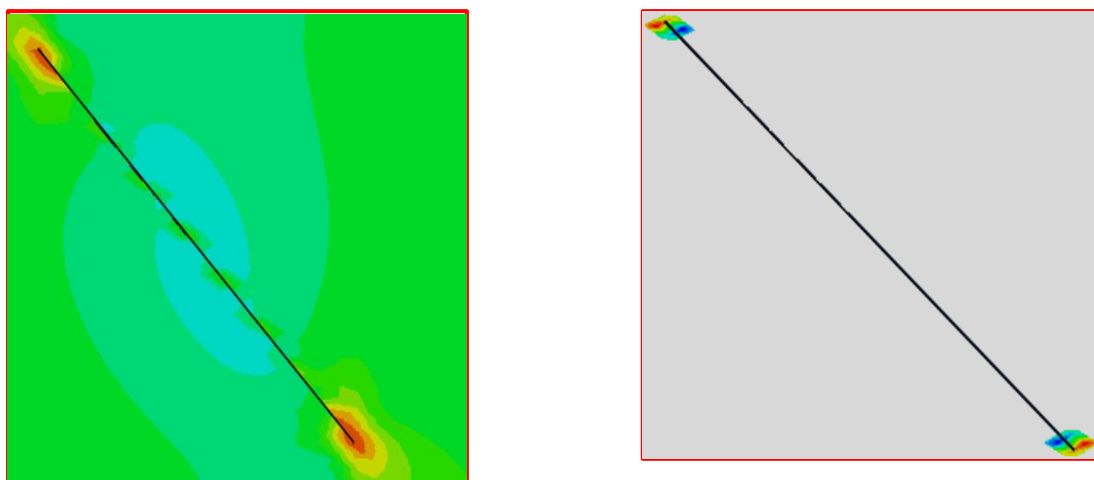


Figure 4. 14 Crack propagation analyzed using the numerical method by applying 622 MPa mean pressure, 45-degree crack angle, and 0.17 coefficient of surface friction

The analytical and experimental results show that the crack, which initiated with a mean pressure of 591 MPa (based on the mean approach), and the propagation pressure is expected to be higher than this value. So that cracks were nucleated (in the austenite) and propagated in the austenite and martensite microstructures (total length about 40 micrometers) at the test pressure of 622 MPa. And also, the depth of the crack that is located is about 60  $\mu\text{m}$ . Again, the initial crack position and its propagation at the applied load of 622 MPa and 0.17 coefficient of friction were analyzed using the numerical approach. Numerical results using the ABAQUS standard show that the maximum stress concentration is observed at depth of  $z = 97 \mu\text{m}$ , cracks propagated (the total length of 27.973 Micro Meters considering the mean property of the austenite and martensite) when the pressure is 622 MPa. The variation of crack length determined using the numerical tools and observed after the experimental test may relate with the combined effect of the initial crack angle and surface characteristics that affects crack growth as discussed above. Also, the distribution of material phases can affect the growth of the crack. For instance, crack nucleate in the austenite and propagates to the left and right direction of the figure until it is blocked by the martensitic microstructure. Therefore, crack is propagated in the mixed area (austenite and martensite) about 27.973 micrometers as predicted by the numerical model. Table 4.2 describes the error percentage of crack propagation.

**Table 4. 2 Error percentage of crack propagation**

Parameters	Magnitude	Initial crack length	Propagated crack length	Experimental crack length	Error in percentage
Applying pressure	550 MPa	10 $\mu\text{m}$	38.2 $\mu\text{m}$	40 $\mu\text{m}$	4.5%
	622 MPa	10 $\mu\text{m}$	38.4 $\mu\text{m}$	40 $\mu\text{m}$	4%
	700 MPa	10 $\mu\text{m}$	39.3 $\mu\text{m}$	40 $\mu\text{m}$	1.7%5
Coefficient of Surface friction	0	10 $\mu\text{m}$	38.4 $\mu\text{m}$	40 $\mu\text{m}$	4%
	0.01	10 $\mu\text{m}$	37.5 $\mu\text{m}$	40 $\mu\text{m}$	6.2%5
	0.17	10 $\mu\text{m}$	36.92 $\mu\text{m}$	40 $\mu\text{m}$	7.7%
The angle of crack inclination	25°	10 $\mu\text{m}$	37.3 $\mu\text{m}$	40 $\mu\text{m}$	6.75%
	45°	10 $\mu\text{m}$	38.6 $\mu\text{m}$	40 $\mu\text{m}$	3.5%
	75°	10 $\mu\text{m}$	36.7 $\mu\text{m}$	40 $\mu\text{m}$	8.25%

In this paper Crack propagation analyzed using the numerical method by applying 622 MPa mean pressure, 45-degree crack angle, and 0.17 coefficient of surface friction has

$$\text{average error} = \frac{4\%+7.7\%+3.5\%}{3} = 5.067\%$$

That means The Abaqus result propagated with the crack length of 37.973  $\mu\text{m}$  and when compared to the experimental crack length has a percentage of error of 5.067%

## CHAPTER - 5 CONCLUSIONS AND RECOMMENDATIONS

### 5.1 Conclusion

This paper investigates the effect of load, crack angle, and surface friction on the propagation subsurface crack in the through-hardened steel subjected under rolling sliding contact. Besides the effect of these parameters on the equivalent stress distribution and depth of maximum stress was evaluated using an Extended Finite Element Method (XFEM) in the Abaqus tool. Extended Finite Element Method (XFEM) in recent years become an efficient method to analyze crack propagation problems without the need to modify the mesh generated successively. The results of the Numerical analysis of Subsurface Crack Propagation in Through-Hardened Steel Subjected under Rolling–Sliding depending on the applied boundary conditions, crack angle, coefficient of friction, and applied load. The numerical results lead to the following conclusions:

- The material for a mean pressure of 622 MPa causes cracks to propagate to 37.973 $\mu$ m.
- The behavior of crack is mode II behavior.
- When we increase the coefficient of friction the maximum stress goes to the surface from the maximum depth (Z) and decreases the coefficient friction reaches maximum shear stress to the maximum depth Z. The FEM results obtained are physically similar to experimental data that previously done

### 5.2 Recommendation

Crack initiation and propagation are unpredictable, complicated, and high-cycle processes. so, to minimize this damage there should be a regular schedule for maintenance and correction maintenance. Based on the result of this paper the following recommendation is useful.

- Using XFEM for crack propagation analysis, which has become a very important generalization of classical finite element technique to reduce the drawbacks of the solutions' mesh dependencies by developing mesh-independent solutions.
- Studying the crack at various friction and load coefficients that it used to know at what load the crack starts to expand and at which friction coefficient we get the maximum value
- Use to research the crack with different angles of inclination helps to understand at which angle we get maximum propagation and stress.

### **5.3 Future work**

There are some gaps found during the study of this thesis work, in numerical modeling of subsurface crack propagation under rolling sliding contact that necessary for future work. Additional deeper study research is required to fill these gaps. Further studies require on

- Understanding the effect of the material's microstructure on fatigue life cracks initiation and propagation.
- Understanding Lubricant effect on the initiation and propagation of cracks as well as experimental validation
- The Effect of 3D Modelling of crack initiation and propagation under rolling sliding contact

## REFERENCES

- [1] F. Sadeghi and P. C. Sui, "Subsurface Stresses in Rolling/Sliding Machine Components," p. 11.
- [2] J. H. Melson, "Fatigue Crack Growth Analysis with Finite Element Methods and a Monte Carlo Simulation," p. 160.
- [3] L. Xin, V. L. Markine, and I. Y. Shevtsov, "Numerical analysis of the dynamic interaction between wheel set and turnout crossing using the explicit finite element method," p. 28.
- [4] H. M. El-sayed, M. Lotfy, H. N. El-din Zohny, and H. S. Riad, "Prediction of fatigue crack initiation life in railheads using finite element analysis," *Ain Shams Eng. J.*, vol. 9, no. 4, pp. 2329–2342, Dec. 2018, doi: 10.1016/j.asej.2017.06.003.
- [5] C.-M. Everitt and B. Alfredsson, "Surface initiation of rolling contact fatigue at asperities considering slip, shear limit and thermal elastohydrodynamic lubrication," *Tribol. Int.*, vol. 137, pp. 76–93, Sep. 2019, doi: 10.1016/j.triboint.2019.04.023.
- [6] M. Ghodrati, M. Ahmadian, and R. Mirzaeifar, "Modeling of rolling contact fatigue in rails at the microstructural level," *Wear*, vol. 406–407, pp. 205–217, Jul. 2018, doi: 10.1016/j.wear.2018.04.016.
- [7] Y. Kadin and A. V. Rychahivskyy, "Modeling of surface cracks in rolling contact," *Mater. Sci. Eng. A*, vol. 541, pp. 143–151, Apr. 2012, doi: 10.1016/j.msea.2012.02.016.
- [8] S. Tesfaye Mekonone, W. Pahl, and A. Molinari, "Influence of the microstructure on the subsurface and surface damage during lubricated rolling–sliding wear of sintered and sinterhardened 1.5%Mo–2%Cu–0.6%C steel: theoretical analysis and experimental investigation," *Powder Metall.*, vol. 61, no. 3, pp. 187–196, May 2018, doi: 10.1080/00325899.2018.1446706.
- [9] P. R. Anoopnath, V. Suresh Babu, and A. K. Vishwanath, "Hertz Contact Stress of Deep Groove Ball Bearing," *Mater. Today Proc.*, vol. 5, no. 2, pp. 3283–3288, 2018, doi: 10.1016/j.matpr.2017.11.570.
- [10] J. Zhao, F. Sadeghi, and H. M. Nixon, "A Finite Element Analysis of Surface Pocket Effects in Hertzian Line Contact," *J. Tribol.*, vol. 122, no. 1, pp. 47–54, Jan. 2000, doi: 10.1115/1.555328.
- [11] Usman and S.-C. Huang, "The study of stresses characteristic of contact mechanism in total knee replacement using two-dimensional finite element analysis," *Biomed. Mater. Eng.*, vol. 28, no. 5, pp. 567–578, Aug. 2017, doi: 10.3233/BME-171688.
- [12] R. Ledesma-Alonso, E. Raphaël, L. Léger, F. Restagno, and C. Poulard, "Stress concentration in periodically rough Hertzian contact: Hertz to soft-flat-punch transition," *Proc. R. Soc. Math. Phys. Eng. Sci.*, vol. 472, no. 2193, p. 20160235, Sep. 2016, doi: 10.1098/rspa.2016.0235.
- [13] X. Hua, B. M. Wroblewski, Z. Jin, and L. Wang, "The effect of cup inclination and wear on the contact mechanics and cement fixation for ultra high molecular weight polyethylene total hip replacements," *Med. Eng. Phys.*, vol. 34, no. 3, pp. 318–325, Apr. 2012, doi: 10.1016/j.medengphy.2011.07.026.
- [14] Z.-Q. Gong and K. Komvopoulos, "Effect of Surface Patterning on Contact Deformation of Elastic-Plastic Layered Media," *J. Tribol.*, vol. 125, no. 1, pp. 16–24, Jan. 2003, doi: 10.1115/1.1501086.
- [15] W. Wang, H. Wen, N. He, and W. Chen, "Effect of load on tribological properties of silicon nitride/steel under rolling-sliding contact condition," *Tribol. Int.*, vol. 125, pp. 27–38, Sep. 2018, doi: 10.1016/j.triboint.2018.04.022.
- [16] T. Bruce, H. Long, and R. S. Dwyer-Joyce, "Threshold Maps for Inclusion-Initiated Micro-Cracks and White Etching Areas in Bearing Steel: The Role of Impact Loading and Surface Sliding," *Tribol. Lett.*, vol. 66, no. 3, p. 111, Sep. 2018, doi: 10.1007/s11249-018-1068-0.

- [17] M. Khajeh Salehani, N. Irani, and L. Nicola, “Modeling adhesive contacts under mixed-mode loading,” *J. Mech. Phys. Solids*, vol. 130, pp. 320–329, Sep. 2019, doi: 10.1016/j.jmps.2019.06.010.
- [18] D. I. Fletcher and J. H. Beynon, “The effect of contact load reduction on the fatigue life of pearlitic rail steel in lubricated rolling-sliding contact,” *Fatigue Htmlemt Glyphamp Asciiamp Fract. Eng. Mater. Struct.*, vol. 23, no. 8, pp. 639–650, Aug. 2000, doi: 10.1046/j.1460-2695.2000.00275.x.
- [19] B. J. Briscoe and F. Motamedi, “The ballistic impact characteristics of aramid fabrics: the influence of in&face friction,” p. 19.
- [20] G. Styles, R. Rahmani, H. Rahnejat, and B. Fitzsimons, “In-cycle and life-time friction transience in piston ring–liner conjunction under mixed regime of lubrication,” *Int. J. Engine Res.*, vol. 15, no. 7, pp. 862–876, Oct. 2014, doi: 10.1177/1468087413519783.
- [21] D. E. Sander, H. Allmaier, H. H. Priebsch, M. Witt, and A. Skiadas, “Simulation of journal bearing friction in severe mixed lubrication – Validation and effect of surface smoothing due to running-in,” *Tribol. Int.*, vol. 96, pp. 173–183, Apr. 2016, doi: 10.1016/j.triboint.2015.12.024.
- [22] B. N. J. Persson, “Theory of rubber friction and contact mechanics,” *J. Chem. Phys.*, vol. 115, no. 8, pp. 3840–3861, Aug. 2001, doi: 10.1063/1.1388626.
- [23] Y. Peng *et al.*, “The friction and wear properties of steel wire rope sliding against itself under impact load,” *Wear*, vol. 400–401, pp. 194–206, Apr. 2018, doi: 10.1016/j.wear.2018.01.010.
- [24] W. M. da Silva, H. L. Costa, and J. D. B. de Mello, “Transitions in abrasive wear mechanisms: Effect of the superimposition of interactions,” *Wear*, vol. 271, no. 5–6, pp. 977–986, Jun. 2011, doi: 10.1016/j.wear.2011.04.010.
- [25] Z. Hu, W. Lu, M. D. Thouless, and J. R. Barber, “Effect of plastic deformation on the evolution of wear and local stress fields in fretting,” *Int. J. Solids Struct.*, vol. 82, pp. 1–8, Mar. 2016, doi: 10.1016/j.ijsolstr.2015.12.031.
- [26] S. Fouvry, Ph. Kapsa, L. Vincent, and K. Dang Van, “Theoretical analysis of fatigue cracking under dry friction for fretting loading conditions,” *Wear*, vol. 195, no. 1–2, pp. 21–34, Jul. 1996, doi: 10.1016/0043-1648(95)06741-8.
- [27] W. Cao, W. Pu, J. Wang, and K. Xiao, “Effect of contact path on the mixed lubrication performance, friction and contact fatigue in spiral bevel gears,” *Tribol. Int.*, vol. 123, pp. 359–371, Jul. 2018, doi: 10.1016/j.triboint.2018.03.015.
- [28] S.-C. Vlădescu, A. V. Olver, I. G. Pegg, and T. Reddyhoff, “Combined friction and wear reduction in a reciprocating contact through laser surface texturing,” *Wear*, vol. 358–359, pp. 51–61, Jul. 2016, doi: 10.1016/j.wear.2016.03.035.
- [29] K. W. Liew, C. K. Kok, and M. N. Ervina Efzan, “Effect of EDM dimple geometry on friction reduction under boundary and mixed lubrication,” *Tribol. Int.*, vol. 101, pp. 1–9, Sep. 2016, doi: 10.1016/j.triboint.2016.03.029.
- [30] O. Elomaa, V. K. Singh, A. Iyer, T. J. Hakala, and J. Koskinen, “Graphene oxide in water lubrication on diamond-like carbon vs. stainless steel high-load contacts,” *Diam. Relat. Mater.*, vol. 52, pp. 43–48, Feb. 2015, doi: 10.1016/j.diamond.2014.12.003.
- [31] S. C. Bellemare, M. Dao, and S. Suresh, “Effects of mechanical properties and surface friction on elasto-plastic sliding contact,” *Mech. Mater.*, vol. 40, no. 4–5, pp. 206–219, Apr. 2008, doi: 10.1016/j.mechmat.2007.07.006.
- [32] A. Papangelo and M. Ciavarella, “On mixed-mode fracture mechanics models for contact area reduction under shear load in soft materials,” *J. Mech. Phys. Solids*, vol. 124, pp. 159–171, Mar. 2019, doi: 10.1016/j.jmps.2018.10.011.
- [33] D. Ne’lias *et al.*, “Role of Inclusions, Surface Roughness and Operating Conditions on Rolling Contact Fatigue,” *J. Tribol.*, vol. 121, no. 2, pp. 240–251, Apr. 1999, doi: 10.1115/1.2833927.

- [34] E. Demir and D. Raabe, "Mechanical and microstructural single-crystal Bauschinger effects: Observation of reversible plasticity in copper during bending," *Acta Mater.*, vol. 58, no. 18, pp. 6055–6063, Oct. 2010, doi: 10.1016/j.actamat.2010.07.023.
- [35] T. T. Nguyen, J. Yvonnet, Q.-Z. Zhu, M. Bornert, and C. Chateau, "A phase field method to simulate crack nucleation and propagation in strongly heterogeneous materials from direct imaging of their microstructure," *Eng. Fract. Mech.*, vol. 139, pp. 18–39, May 2015, doi: 10.1016/j.engfracmech.2015.03.045.
- [36] D.-K. Leu, "Modeling of surface roughness effect on dry contact friction in metal forming," *Int. J. Adv. Manuf. Technol.*, vol. 57, no. 5–8, pp. 575–584, Nov. 2011, doi: 10.1007/s00170-011-3305-7.
- [37] N. Erarslan, "Microstructural investigation of subcritical crack propagation and Fracture Process Zone (FPZ) by the reduction of rock fracture toughness under cyclic loading," *Eng. Geol.*, vol. 208, pp. 181–190, Jun. 2016, doi: 10.1016/j.enggeo.2016.04.035.
- [38] M. Epstein and A. Roychowdhury, "Embedded homogeneity of beams in the nonlinear domain," *Int. J. Solids Struct.*, vol. 58, pp. 201–206, Apr. 2015, doi: 10.1016/j.ijsolstr.2015.01.004.
- [39] K. R. Gratz, B. L. Wong, W. C. Bae, and R. L. Sah, "The effects of focal articular defects on cartilage contact mechanics," *J. Orthop. Res.*, vol. 27, no. 5, pp. 584–592, May 2009, doi: 10.1002/jor.20762.
- [40] L. Galda, J. Sep, and S. Prucnal, "The effect of dimples geometry in the sliding surface on the tribological properties under starved lubrication conditions," *Tribol. Int.*, vol. 99, pp. 77–84, Jul. 2016, doi: 10.1016/j.triboint.2016.03.015.
- [41] F. Restagno, J. Crassous, C. Cottin-Bizonne, and E. Charlaix, "Adhesion between weakly rough beads," *Phys. Rev. E*, vol. 65, no. 4, p. 042301, Apr. 2002, doi: 10.1103/PhysRevE.65.042301.
- [42] M. I. Lashhab, G. A. Rogerson, and K. J. Sandiford, "Dispersion phenomena in symmetric pre-stressed layered elastic structures," *Int. J. Solids Struct.*, vol. 58, pp. 220–232, Apr. 2015, doi: 10.1016/j.ijsolstr.2015.01.006.
- [43] W. J. Qin and C. Y. Guan, "An investigation of contact stresses and crack initiation in spur gears based on finite element dynamics analysis," *Int. J. Mech. Sci.*, vol. 83, pp. 96–103, Jun. 2014, doi: 10.1016/j.ijmecsci.2014.03.035.
- [44] F. Shen and K. Zhou, "An elasto-plastic-damage model for initiation and propagation of spalling in rolling bearings," *Int. J. Mech. Sci.*, vol. 161–162, p. 105058, Oct. 2019, doi: 10.1016/j.ijmecsci.2019.105058.
- [45] S. Ancellotti, M. Benedetti, M. Dallago, and V. Fontanari, "Fluid Pressurization and Entrapment Effects on the SIFs of Cracks produced under lubricated Rolling-Sliding Contact Fatigue," *Procedia Struct. Integr.*, vol. 2, pp. 3098–3108, 2016, doi: 10.1016/j.prostr.2016.06.387.
- [46] M. Sraml, "Numerical procedure for predicting the rolling contact fatigue crack initiation," *Int. J. Fatigue*, vol. 25, no. 7, pp. 585–595, Jul. 2003, doi: 10.1016/S0142-1123(03)00019-7.
- [47] R. Raga, I. Khader, C. Zdeněk, and A. Kailer, "Experimental and numerical investigation of crack initiation and propagation in silicon nitride ceramic under rolling and cyclic contact," *J. Phys. Conf. Ser.*, vol. 843, p. 012030, May 2017, doi: 10.1088/1742-6596/843/1/012030.
- [48] R. Potočník, J. Flašker, B. Zafošnik, and S. Glodež, "The Parametric Study of the Crack Growth in the Lubricated Rolling-Sliding Contact Problems," *Key Eng. Mater.*, vol. 348–349, pp. 689–692, Sep. 2007, doi: 10.4028/www.scientific.net/KEM.348-349.689.
- [49] S. Ancellotti, M. Benedetti, M. Dallago, and V. Fontanari, "The role of the second body on the pressurization and entrapment of oil in cracks produced under lubricated rolling-sliding contact fatigue," *Theor. Appl. Fract. Mech.*, vol. 91, pp. 3–16, Oct. 2017, doi: 10.1016/j.tafmec.2017.02.007.
- [50] Y. Ding and J. A. Gear, "Spalling depth prediction model," *Wear*, vol. 267, no. 5–8, pp. 1181–1190, Jun. 2009, doi: 10.1016/j.wear.2008.12.064.

- [51] J. Ringsberg, "Prediction of fatigue crack initiation for rolling contact fatigue," *Int. J. Fatigue*, vol. 22, no. 3, pp. 205–215, Mar. 2000, doi: 10.1016/S0142-1123(99)00125-5.
- [52] K. Aslantaş and S. Taşgetiren, "Modelling of spall formation in a plate made of austempered ductile iron having a subsurface-edge crack," *Comput. Mater. Sci.*, vol. 29, no. 1, pp. 29–36, Jan. 2004, doi: 10.1016/S0927-0256(03)00091-0.
- [53] G. Fajdiga and M. Sraml, "Fatigue crack initiation and propagation under cyclic contact loading," *Eng. Fract. Mech.*, vol. 76, no. 9, pp. 1320–1335, Jun. 2009, doi: 10.1016/j.engfracmech.2009.02.005.
- [54] K. Aslantaş and S. Taşgetiren, "A study of spur gear pitting formation and life prediction," *Wear*, vol. 257, no. 11, pp. 1167–1175, Dec. 2004, doi: 10.1016/j.wear.2004.08.005.
- [55] G. Fajdiga, S. Glodež, and J. Kramar, "Pitting formation due to surface and subsurface initiated fatigue crack growth in contacting mechanical elements," *Wear*, vol. 262, no. 9–10, pp. 1217–1224, Apr. 2007, doi: 10.1016/j.wear.2006.11.016.
- [56] P. Rycerz, A. Olver, and A. Kadiric, "Propagation of surface initiated rolling contact fatigue cracks in bearing steel," *Int. J. Fatigue*, vol. 97, pp. 29–38, Apr. 2017, doi: 10.1016/j.ijfatigue.2016.12.004.
- [57] K. Zhou and R. Wei, "Modeling cracks and inclusions near surfaces under contact loading," *Int. J. Mech. Sci.*, vol. 83, pp. 163–171, Jun. 2014, doi: 10.1016/j.ijmecsci.2014.03.028.
- [58] D. Zeng *et al.*, "Investigation of the crack initiation of subsurface rolling contact fatigue in railway wheels," *Int. J. Fatigue*, vol. 130, p. 105281, Jan. 2020, doi: 10.1016/j.ijfatigue.2019.105281.
- [59] Y. Yin, Y.-X. Chen, and L. Liu, "Lifetime prediction for the subsurface crack propagation using three-dimensional dynamic FEA model," *Mech. Syst. Signal Process.*, vol. 87, pp. 54–70, Mar. 2017, doi: 10.1016/j.ymsp.2016.09.033.
- [60] N. Weinzapfel and F. Sadeghi, "Numerical modeling of sub-surface initiated spalling in rolling contacts," *Tribol. Int.*, vol. 59, pp. 210–221, Mar. 2013, doi: 10.1016/j.triboint.2012.03.006.
- [61] A. Ghosh, N. Paulson, and F. Sadeghi, "A fracture mechanics approach to simulate sub-surface initiated fretting wear," *Int. J. Solids Struct.*, vol. 58, pp. 335–352, Apr. 2015, doi: 10.1016/j.ijsolstr.2014.11.026.
- [62] Y. Liu, L. Liu, and S. Mahadevan, "Analysis of subsurface crack propagation under rolling contact loading in railroad wheels using FEM," *Eng. Fract. Mech.*, vol. 74, no. 17, pp. 2659–2674, Nov. 2007, doi: 10.1016/j.engfracmech.2007.02.012.
- [63] P. C. Bastias, G. T. Hahn, and C. A. Rubin, "Finite element modelling of subsurface mode II cracks under contact loads," *Eng. Fract. Mech.*, vol. 33, no. 1, pp. 143–152, Jan. 1989, doi: 10.1016/0013-7944(89)90062-3.
- [64] J. Flasker, "Numerical simulation of surface pitting due to contact loading," *Int. J. Fatigue*, vol. 23, no. 7, pp. 599–605, Aug. 2001, doi: 10.1016/S0142-1123(01)00020-2.
- [65] S. Chen, M. Zang, D. Wang, S. Yoshimura, and T. Yamada, "Numerical analysis of impact failure of automotive laminated glass: A review," *Compos. Part B Eng.*, vol. 122, pp. 47–60, Aug. 2017, doi: 10.1016/j.compositesb.2017.04.007.